

# Complex dynamical properties of coupled Van der Pol-Duffing oscillators with balanced loss and gain

Puspendu Roy\* and Pijush K. Ghosh†‡

Department of Physics, Siksha-Bhavana,  
Visva-Bharati University,  
Santiniketan, PIN 731 235, India.

## Abstract

We consider a Hamiltonian system of coupled Van der Pol-Duffing(VdPD) oscillators with balanced loss and gain. The system is analyzed perturbatively by using Renormalization Group(RG) techniques as well as Multiple Scale Analysis(MSA). Both the methods produce identical results in the leading order of the perturbation. The RG flow equation is exactly solvable and the slow variation of amplitudes and phases in time can be computed analytically. The system is analyzed numerically and shown to admit periodic solutions in regions of parameter-space, confirming the results of the linear stability analysis and perturbation methods. The complex dynamical behavior of the system is studied in detail by using time-series, Poincaré-sections, power-spectra, auto-correlation function and bifurcation diagrams. The Lyapunov exponents are computed numerically. The numerical analysis reveals chaotic behaviour in the system beyond a critical value of the parameter that couples the two VdPD oscillators through linear coupling, thereby providing yet another example of Hamiltonian chaos in a system with balanced loss and gain. Further, we modify the non-linear terms of the model to make it a non-Hamiltonian system of coupled VdPD oscillators with balanced loss and gain. The non-Hamiltonian system is analyzed perturbatively as well as numerically and shown to possess regular periodic as well as chaotic solutions. It is seen that the  $\mathcal{PT}$ -symmetry is not an essential requirement for the existence of regular periodic solutions in both the Hamiltonian as well as non-Hamiltonian systems.

**Keywords:** System with balanced loss and gain, Van der Pol-Duffing oscillator, Chaos, Multiple Scale Analysis, Renormalization Group Techniques

---

\***email:**puspenduroy716@gmail.com

†**email:** pijushkanti.ghosh@visva-bharati.ac.in

‡Corresponding Author

# 1 Introduction

Systems with balanced loss and gain have received considerable interests over the last few years[1]. One of the characteristic features of such a system is that the flow preserves the volume in the position-velocity state space, although the individual degrees of freedom are subjected to loss or gain[1]. The system is non-dissipative and may admit periodic solutions within some regions in the parameter-space. The Hamiltonian formulation is possible for suitable choice of the potential and the corresponding quantum theory is well defined within appropriate Stoke wedges[2]. The mathematical model[2] for an experimentally realized  $\mathcal{PT}$ -symmetric coupled resonators[3] provides a prototype for a system with balanced loss and gain that incorporates all these features. The periodic solutions and the quantum bound states exist only in the  $\mathcal{PT}$ -symmetric phase. The phase-transition from  $\mathcal{PT}$ -symmetric to  $\mathcal{PT}$ -broken phase is accompanied by a change in the nature of the solution, namely, the bounded solution becomes unbounded. This observation has generated some interest and lead to introduction of many  $\mathcal{PT}$ -symmetric Hamiltonian systems with balanced loss and gain[4, 5, 6, 7, 8, 9, 10, 11]. The examples of Hamiltonian system with balanced loss and gain include systems with nonlinear interaction[5, 6, 7, 8, 9, 10], many-particle systems[4, 8, 9, 10], systems with space-dependent loss-gain terms[9], systems with Lorentz interaction[11] etc..

It has been shown recently that non- $\mathcal{PT}$  symmetric systems with balanced loss and gain may also admit periodic solutions —the requirement of  $\mathcal{PT}$ -symmetry is not necessary[12]. The most general form of parity transformation that is embedded in the generic Lorentz transformation is considered to check the symmetry of these non- $\mathcal{PT}$  symmetric systems. This is consistent with the present understanding that the  $CPT$ -symmetry of  $\mathcal{PT}$ -symmetric quantum systems is expected to correspond to the  $CPT$ -theorem[13] of a local Lorentz-invariant field theory at a more fundamental level. It may be noted that the  $CPT$  theorem, which was originally derived for a hermitian Hamiltonian, has now been extended to the case of non-hermitian Hamiltonian[14]. Further, there is no signature of violation of Lorentz invariance in nature so far and the  $CPT$  is considered to be a fundamental symmetry of nature. This justifies the consideration of only linear transformation to describe parity operation for a classical system. This is also not in contradiction with the corresponding quantum theory, since the parity and time-reversal operators are not unique for a quantum system[1].

The example of a non- $\mathcal{PT}$  symmetric mechanical system with balanced loss-gain that admits periodic solution is described by a Duffing oscillator coupled to an anti-damped oscillator with a variable angular frequency[12]. The Hamiltonian describes a multi-stable system with very rich dynamical behaviour. It exhibits regular periodic solutions within regions of the parameter-space. The chaotic behaviour is observed in the system beyond a critical value of the parameter that couples the Duffing oscillator to the anti-damped harmonic oscillator, thereby providing the first example of Hamiltonian chaos in a system with balanced loss and gain. The system contains positional non-conservative forces[15] or curl-forces[16] which are known to admit chaotic behaviour. The standard Duffing oscillator exhibits chaotic behaviour only if an external forcing term is added to the system. Further, the system is non-Hamiltonian. On the other hand, there is no external forcing term in the coupled Duffing oscillator model with balanced loss and gain. The term that couples to the anti-damped oscillator may be interpreted as the forcing term.

The Van der Pol oscillator is a prototype for systems with self-excited limit cycle oscillations. The equation has been used to model oscillations in vacuum tube triode circuit[17], biology[18, 19], phonation[20], seismology[21], quantum synchronisation[22], quantum criticality[23] etc. The Van der Pol equation is nonlinear due to the space-dependent gain/loss coefficient which makes it damped in one region of space and anti-damped in the remaining part of the line. If a nonlinear restoring force with cubic nonlinearity is added to the system in addition to the linear restoring

force, a double-well potential is obtained and the system is known as VdPD oscillator[24, 25, 26, 27, 28, 29]. The dynamical behaviour of the system is quite rich depending on different phases of the double-well potential[27]. The VdPD has been studied extensively in the context of convective instability of a binary fluid mixture in a porous medium[24], hydrodynamics[25], analog electronic system[26], bifurcation and chaos[27], integrability[28, 29]. Various models of coupled Van der Pol oscillators[30, 31] and coupled VdPD oscillators[32] have also been considered.

The purpose of this article is to study systems of coupled VdPD oscillators with balanced loss and gain. We present two different non- $\mathcal{PT}$ -symmetric models of coupled VdPD oscillators of which one is a Hamiltonian system and the other one non-Hamiltonian. The Hamiltonian system is a generalization of the coupled Duffing oscillator model[12] by making the balanced loss-gain terms space-dependent. The two oscillators are coupled via loss-gain terms in addition to coupling through the potential terms. The space-dependence of the loss-gain terms is such that one of the oscillators is dissipative within an elliptic region and anti-damped in the remaining part of the configuration space. The requirement of balanced loss-gain terms necessitates exactly opposite behaviour for the second oscillator. The non-Hamiltonian system describes two coupled VdPD oscillators with the same space-dependent loss-gain terms. This model is a generalization of non- $\mathcal{PT}$ -symmetric non-Hamiltonian coupled Duffing oscillators with constant balanced loss-gain[1, 33].

We analyze the Hamiltonian system perturbatively by using MSA[34] and RG[35] methods. The results in the leading order of the perturbation are identical for both the methods. The RG flow equation defines a dimer model in which the two modes are coupled nonlinearly through the balanced loss-gain terms along with coupling via nonlinear interaction. The RG flow equation is exactly solvable and the slow variation of the amplitudes and the phases are determined analytically. The system admits regular periodic solutions within regions of parameter-space which are confirmed by numerical solutions. Thus, the list of non- $\mathcal{PT}$ -symmetric systems with balanced loss and gain admitting regular periodic solution is enlarged by the inclusion of this model. The numerical investigations reveal chaotic behaviour in these systems beyond some critical value of the linear coupling term. The chaotic behaviour is seen in the standard VdPD oscillator in presence of a driving term. Although the nonlinear oscillator considered in this article is undriven, the chaotic behaviour may be attributed to the coupling between the two degrees of freedom of a given model. The complex dynamical behavior of the systems is investigated numerically by computing time-series, Poincaré-sections, power-spectra, auto-correlation function, bifurcation diagrams and the Lyapunov exponents. We get yet another example of Hamiltonian chaos for systems with balanced loss-gain.

We analyze a second system which differs from the first model in the velocity-independent nonlinear terms. This is a generalization of the non-Hamiltonian system of two coupled Duffing oscillators introduced in [1, 33] by allowing the loss-gain terms to be space-dependent. The model considered in Ref. [33] is  $\mathcal{PT}$ -symmetric and existence of regular periodic solution is attributed to unbroken  $\mathcal{PT}$ -symmetry. The system considered in Ref. [1] admits regular periodic solutions in  $\mathcal{PT}$ -symmetric as well as non- $\mathcal{PT}$ -symmetric regimes and reduces to the model of Ref. [33] in a particular limit. The second model is non-Hamiltonian and analyzed perturbatively as well as numerically. The RG flow equation differs from the first model only in the equation for the phase of one of the modes and is exactly solvable. The system admits regular periodic solution in the  $\mathcal{PT}$ -symmetric as well as non- $\mathcal{PT}$ -symmetric regimes. The systems admits chaotic behaviour which is investigated numerically by computing time-series, Poincaré-sections, power-spectra, auto-correlation function, bifurcation diagrams and the Lyapunov exponents.

The plan of the article is the following. We introduce the Hamiltonian system describing coupled VdPD oscillators in the next section. The general formalism along with  $\mathcal{PT}$ -symmetry and linear stability analysis are presented at the beginning. The equations of motion are analyzed

by using MSA and RG techniques in Secs. 2.2.1 and 2.2.2, respectively. The solutions obtained by these two methods are shown to be identical in the leading order of the perturbation. The RG flow equation is solved in Sec. 2.2.1. The results of numerical investigations are presented in Sec. 2.3 —regular solutions are described in Sec. 2.3.1, while the analysis for chaotic dynamics given in Sec. 2.3.1. The non-Hamiltonian system describing coupled VdPD is introduced in Sec. 3 and the details of numerical investigations are presented in Sec. 3.1. Finally, the results are summarized in Sec. 4.

## 2 Hamiltonian system

The Hamiltonian system is described by the equations of motion,

$$\begin{aligned}\ddot{x} + 2\gamma(1 - rx^2 - sy^2)\dot{x} + \omega^2x + \beta_1y + gx^3 &= 0, \\ \ddot{y} - 2\gamma(1 - rx^2 - sy^2)\dot{y} + \omega^2y + \beta_2x + 3gx^2y &= 0,\end{aligned}\tag{1}$$

where  $\omega$  is the angular frequency corresponding to the linear restoring force,  $\beta_1, \beta_2$  are the strengths of the linear coupling between the two modes and  $g$  is the strength of the nonlinear interaction. The parameter  $\gamma$  is the strength of the constant loss-gain, while  $r$  and  $s$  are strengths of the space-dependent loss-gain terms. The equation  $rx^2 + sy^2 = 1$  corresponds to vanishing loss-gain and separates two regions in the configuration space corresponding to dissipative and anti-damped regions. For  $\gamma > 0$ , the first equation in Eq. (1) is dissipative within the elliptic region  $rx^2 + sy^2 < 1$ , while it is anti-damped for  $rx^2 + sy^2 > 1$ . The Eq. (1) defines a system of balanced loss and gain in the sense that the flow in the position-velocity state space preserves the volume, although individual degrees of freedom are subjected to gain or loss. This is manifested in the second equation which has exactly opposite behaviour in the respective regions of the configuration space in respect to the first equation due to the requirement of balanced loss-gain[11].

There are several interesting limits of the system defined by Eq. (1). The mathematical model[2] describing an experimentally realized  $\mathcal{PT}$ -symmetric coupled resonators[3] is obtained for  $r = s = g = 0, \beta_1 = \beta_2$ . The coupled Duffing oscillators with balanced loss-gain[12] is obtained in the limit  $r = s = 0$ . The  $x$ -degree of freedom decouples completely for  $s = \beta_1 = 0$ , while the  $y$ -degree of freedom is unidirectionally coupled to it. This limit corresponds to Hamiltonian formulation of the standard VdPD oscillator with the  $y$  degree of freedom treated as auxiliary variable. The standard techniques for analyzing a Hamiltonian system like canonical perturbation theory, quantization, KAM theory, integrability etc. may be used to study VdPD oscillator. The canonical perturbation theory has been used successfully[36, 37] for the standard Van der Pol oscillator, i.e,  $s = \beta_1 = g = 0$ .

The equations of motion (1) may be obtained from the Lagrangian,

$$\mathcal{L} = \dot{x}\dot{y} + \gamma \left[ \left( x - \frac{rx^3}{3} - sy^2x \right) \dot{y} - \left( y - rx^2y - \frac{sy^3}{3} \right) \dot{x} \right] - \omega^2xy - \frac{1}{2}(\beta_2x^2 + \beta_1y^2) - gx^3y.$$

The canonical momenta are,

$$P_x = \dot{y} - \gamma \left( y - rx^2y - \frac{sy^3}{3} \right), \quad P_y = \dot{x} + \gamma \left( x - \frac{rx^3}{3} - sy^2x \right),\tag{2}$$

and the Hamiltonian is evaluated as,

$$H = P_xP_y + \gamma \left[ \left( y - rx^2y - \frac{sy^3}{3} \right) P_y - \left( x - \frac{rx^3}{3} - sy^2x \right) P_x \right]$$

$$- \gamma^2 \left( y - rx^2y - \frac{sy^3}{3} \right) \left( x - \frac{rx^3}{3} - sy^2x \right) + \omega^2 xy + \frac{1}{2} (\beta_2 x^2 + \beta_1 y^2) + gx^3y. \quad (3)$$

The Hamiltonian formulation for generic systems with balanced loss-gain is given in Refs. [8, 10] that is used to obtain  $\mathcal{L}$  and  $H$ . The Hamiltonian for the specific case of coupled Van der Pol oscillators, i.e.  $\beta_1 = \beta_2 = g = 0$  was obtained in Ref. [36]. We define the generalized momenta as,

$$\Pi_x = P_x + \gamma A_x, \quad \Pi_y = P_y + \gamma A_y, \quad A_x(x, y) \equiv y - rx^2y - \frac{sy^3}{3}, \quad A_y(x, y) \equiv - \left( x - \frac{rx^3}{3} - sy^2x \right), \quad (4)$$

where  $A_x$  and  $A_y$  may be interpreted as ‘‘fictitious gauge potential’’[10]. The magnetic field corresponding to this fictitious gauge potential is equivalent to the space-dependence of gain-loss terms[10]. If the system is considered in the background of realistic magnetic field, there will be additional contribution to the gauge potentials[11] The Hamiltonian can be rewritten as,

$$H = \Pi_x \Pi_y + V(x, y), \quad V(x, y) \equiv \omega^2 xy + \frac{1}{2} (\beta_2 x^2 + \beta_1 y^2) + gx^3y. \quad (5)$$

In general, the Hamiltonian is not positive-definite.

The independent scales in the system may be fixed by employing the following transformations,

$$t \rightarrow \omega^{-1}t, \quad x \rightarrow |\beta_2|^{-\frac{1}{2}}x, \quad y \rightarrow |\beta_1|^{-\frac{1}{2}}y, \quad \beta_1 \neq 0, \beta_2 \neq 0. \quad (6)$$

The model can be described in terms of five independent parameters  $\Gamma, \beta, \alpha, a$  and  $b$  defined as,

$$\Gamma = \frac{\gamma}{\omega}, \quad \beta = \frac{\sqrt{|\beta_1||\beta_2|}}{\omega^2}, \quad \alpha = \frac{g}{|\beta_2|\omega^2}, \quad a = \frac{r}{|\beta_2|}, \quad b = \frac{s}{|\beta_1|}. \quad (7)$$

The total number of independent parameters is reduced from seven to five and convenient for analyzing the system. The equations of motion have the following expressions:

$$\begin{aligned} \ddot{x} + 2\Gamma(1 - ax^2 - by^2)\dot{x} + x + \text{sgn}(\beta_1) \beta y + \alpha x^3 &= 0, \\ \ddot{y} - 2\Gamma(1 - ax^2 - by^2)\dot{y} + y + \text{sgn}(\beta_2) \beta x + 3\alpha x^2 y &= 0, \end{aligned} \quad (8)$$

where  $\text{sgn}(x)$  is the signum function. The scale transformation (6) implies,

$$\begin{aligned} P_x &\rightarrow \frac{\omega}{\sqrt{\beta_1}} \tilde{P}_x, \quad P_y \rightarrow \frac{\omega}{\sqrt{\beta_2}} \tilde{P}_y, \quad H \rightarrow \beta^{-1} \tilde{H}, \\ \tilde{P}_x &\equiv \dot{y} - \Gamma y \left( 1 - ax^2 - \frac{by^2}{3} \right), \quad \tilde{P}_y \equiv \dot{x} + \Gamma x \left( 1 - \frac{ax^2}{3} - by^2 \right). \end{aligned} \quad (9)$$

Defining generalized momenta  $\tilde{\Pi}_x = \tilde{P}_x + \Gamma y \left( 1 - ax^2 - \frac{by^2}{3} \right)$ ,  $\tilde{\Pi}_y = \tilde{P}_y - \Gamma x \left( 1 - \frac{ax^2}{3} - by^2 \right)$ , the Hamiltonian  $\tilde{H}$  can be rewritten as,

$$\tilde{H} = \tilde{\Pi}_x \tilde{\Pi}_y + V(x, y), \quad V(x, y) = xy + \frac{\beta}{2} [\text{sgn}(\beta_2) x^2 + \text{sgn}(\beta_1) y^2] + \alpha x^3y. \quad (10)$$

The Hamiltonian  $\tilde{H}$  and the equations of motion in (8) will be considered for further analysis and the results in terms of the original variables may be obtained by inverse scale transformations. The Hamiltonian  $\tilde{H}$  or equivalently the energy  $E = \dot{x}\dot{y} + V(x, y)$  is a constant of motion, but

neither semi-positive definite nor bounded from below. The energy may be bounded from below for specific orbits in the phase-space to be determined from the equations of motion.

The parity  $\mathcal{P}$  and time-reversal symmetry  $\mathcal{T}$  in  $2 + 1$  space-time dimensions may be defined as follows:

$$\begin{aligned}\mathcal{T} : t &\rightarrow -t, \quad \tilde{P}_x \rightarrow -\tilde{P}_x, \quad \tilde{P}_y \rightarrow -\tilde{P}_y \\ \mathcal{P} : (x, y) &\rightarrow (y, x), \quad (\tilde{P}_x, \tilde{P}_x) \rightarrow (\tilde{P}_x, \tilde{P}_x).\end{aligned}\quad (11)$$

The system defined by Eq. (8) is  $\mathcal{PT}$  symmetric for  $a = b$ ,  $\text{sgn}(\beta_1) = \text{sgn}(\beta_2)$ ,  $\alpha = 0$  and becomes non- $\mathcal{PT}$ -symmetric if one or more of these conditions are violated. The parity  $\mathcal{P}$  in Eq. (11) belongs to  $O(2)$  transformation and is consistent with the general expectation that  $\mathcal{CP}\mathcal{T}$ -symmetry of  $\mathcal{PT}$ -symmetric quantum systems will correspond to  $\mathcal{CP}\mathcal{T}$  theorem at a more fundamental level[1]. Any possibility of non-linear transformations with the properties of parity operator for which Eq. (8) may be  $\mathcal{PT}$ -symmetric for  $a \neq b$  or  $\alpha \neq 0$  or  $\text{sgn}(\beta)_1 \neq \text{sgn}(\beta)_2$  is discarded for the same reason, since the  $\mathcal{CP}\mathcal{T}$ -theorem dwells on Lorentz transformation which is linear. The linear stability analysis along with numerical investigations show that the system with  $a = b = 0$  does not admit any periodic solution for  $\text{sgn}(\beta_1) = -\text{sgn}(\beta_2)$  [12]. We choose  $\text{sgn}(\beta_1) = \text{sgn}(\beta_2)$  in this article for simplicity and consider the case  $\beta_1 > 0, \beta_2 > 0$ . The results for  $\beta_1 < 0, \beta_2 < 0$  may be reproduced by simply taking  $\beta \rightarrow -\beta$ . We choose  $\alpha \neq 0$  with (i)  $a = b \neq 0$  and (ii)  $a \neq b$  for which the system is necessarily non- $\mathcal{PT}$ -symmetric and will be shown to admit regular periodic solution as well chaotic behaviour.

## 2.1 Linear Stability Analysis

The Hamilton's equations of motion read,

$$\begin{aligned}\dot{x} &= \tilde{\Pi}_y, \quad \dot{y} = \tilde{\Pi}_x, \quad \dot{\tilde{P}}_x = \Gamma(1 - ax^2 - by^2)\tilde{\Pi}_x - 2axy\Gamma\tilde{\Pi}_y - \beta x - y - 3\alpha x^2 y \\ \dot{\tilde{P}}_y &= -\Gamma(1 - ax^2 - by^2)\tilde{\Pi}_y - 2bxy\Gamma\tilde{\Pi}_x - \beta y - x - \alpha x^3.\end{aligned}\quad (12)$$

The equilibrium points and their stability may be analyzed by employing standard techniques. In particular, the equilibrium points are determined by the solutions of the algebraic equations obtained by putting the right hand side of Eq. (12) equal to zero. It should be noted that a Hamiltonian system admits either center i.e. closed orbit in the phase-space surrounding an equilibrium point or hyperbolic point signalling instability[39]. The stable equilibrium point of a Hamiltonian system is necessarily a center and is not asymptotically stable. The system admits five equilibrium points  $P_0, P_1^\pm, P_2^\pm$  in the phase-space  $(x, y, \tilde{P}_x, \tilde{P}_y)$  of the system,

$$\begin{aligned}P_0 &= (0, 0, 0, 0), P_1^\pm = \left(\pm\delta_+, \pm\eta_+, \mp\Gamma\eta_+ \left(1 - a\delta_+^2 - \frac{b\eta_+^2}{3}\right), \pm\Gamma\delta_+ \left(1 - \frac{a\delta_+^2}{3} - b\eta_+^2\right)\right), \\ P_2^\pm &= \left(\pm\delta_-, \pm\eta_-, \mp\Gamma\eta_- \left(1 - a\delta_-^2 - \frac{b\eta_-^2}{3}\right), \pm\Gamma\delta_- \left(1 - \frac{a\delta_-^2}{3} - b\eta_-^2\right)\right),\end{aligned}\quad (13)$$

where  $\delta_\pm$  and  $\eta_\pm$  are defined as follows:

$$\delta_\pm = \frac{1}{\sqrt{3\alpha}} \left[-2 \pm \sqrt{1 + 3\beta^2}\right]^{\frac{1}{2}}, \quad \eta_\pm = -\frac{\delta_\pm}{3\beta} \left[1 \pm \sqrt{1 + 3\beta^2}\right].\quad (14)$$

We denote the coordinates of a generic equilibrium point in the phase-space as  $Z_0 \equiv (x_0, y_0, \tilde{P}_{x_0}, \tilde{P}_{y_0})$ . The expressions for the coordinates of a given equilibrium point may be obtained from Eqs.

(13,14). The critical points of the Hamiltonian  $\tilde{H}$  are also equilibrium points for the Eq. (12), since both are determined from the equation  $\tilde{H}_Z \equiv \frac{\partial \tilde{H}}{\partial Z} = 0, Z \equiv (x, y, \tilde{P}_x, \tilde{P}_y)$ . The Dirichlet theorem[38] states that a critical point is stable if the Hessian  $\tilde{H}_{ZZ}$  at that point is definite —no conclusion can be drawn for an indefinite Hessian. It has been shown in Ref. [12] that  $\tilde{H}_{ZZ}$  for  $a = b = 0$  is not definite at  $P_0$  and the decision for its stability is inconclusive. This results holds for  $a \neq 0 \neq b$ , since  $\tilde{H}_{ZZ}$  evaluated at  $P_0$  is same for both the cases. Thus, the eigenvalues of  $\tilde{H}_{ZZ}$  do not depend on  $a$  and  $b$ . A similar analysis for the points  $P_1^\pm$  and  $P_2^\pm$  are cumbersome and not attempted in this article. We employ linear stability analysis and numerical investigations to explore the stability of these points. The equilibrium points of a Hamiltonian system are either center or hyperbolic points.

The linear stability analysis of Eq. (12) for  $a = 0 = b$  has been analyzed in detail in Ref. [12]. We observe that the effect of non-zero  $a, b$  is absent for the Point  $P_0$ . The effect on the remaining points  $P_1^\pm, P_2^\pm$  is merely to shift the coordinates  $\tilde{P}_{x_0}, \tilde{P}_{y_0}$  by keeping the coordinates  $x_0, y_0$  unchanged. The criteria for linear stability of an equilibrium point do not depend on the non-linear terms, i.e. the terms with the coefficients  $a, b, \alpha$ . This may be seen by considering small fluctuations around an equilibrium point in the phase space as  $(x = x_0 + \xi_1, y = y_0 + \xi_2, \tilde{P}_x = \tilde{P}_{x_0} + \xi_3, \tilde{P}_y = \tilde{P}_{y_0} + \xi_4)$ . We obtain an equation of the form  $\dot{\xi} = M\xi$  by keeping only the terms linear in  $\xi_i$  in Eq. (12), where  $\xi$  is a vector with four components  $\xi_i$  and  $M$  is a  $4 \times 4$  constant matrix whose eigenvalues determine the stability of small fluctuations around an equilibrium point. The matrix  $M$  is independent of  $P_{x_0}$  and  $P_{y_0}$  and so is its eigenvalues[12]. Thus, the stability criteria are independent of whether  $a, b$  are vanishing or not. We state the results from Ref. [12] for completeness.

**Point  $P_0$ :** The point is an equilibrium point for any  $\alpha$  and  $\beta \neq 0$ . The solutions are stable in a region of the parameter-space defined by the conditions,

$$-\frac{1}{\sqrt{2}} < \Gamma < \frac{1}{\sqrt{2}}, \quad 4\Gamma^2(1 - \Gamma^2) < \beta^2 < 1. \quad (15)$$

**Point  $P_1^\pm$ :** The equilibrium points exist for  $\alpha > 0, \beta^2 > 1$  and  $\alpha < 0, 0 < \beta^2 < 1$ . The expressions for the co-ordinates in the phase-space becomes complex if the above conditions are not satisfied. The stable solutions are obtained in the region  $\alpha > 0$  for  $\beta^2 > 1, \Gamma^2 \leq \frac{\sqrt{2}-1}{\sqrt{2}}$ . The point is unstable  $\alpha < 0, 0 < \beta^2 < 1$ .

**Point  $P_2^\pm$ :** The equilibrium points exist for  $\alpha < 0, 0 < \beta^2 < 1, \beta^2 > 1$ ; otherwise, the co-ordinates become complex. None of the points are stable.

This is a multi-stable system —three out of five equilibrium points are stable.

## 2.2 Perturbative Solution

In this section, the Hamiltonian of two coupled VdPD oscillators with balanced loss and gain is analyzed by perturbative methods. The standard perturbation technique fails due to the appearance of secular terms. The Poincaré-Lindstedt method is also problematic for systems with multiple time-scales. The MSA perturbation method can be applied successfully to a host of nonlinear equations except for systems with hidden time-scales varying with non-integer powers of the perturbation-parameter —the Mathieu equation being one such example[35]. The RG technique is free from this problem, since no time-scale is assumed a priori and it is determined by the flow equations. We analyze the system perturbatively by using RG techniques as well as MSA method. We find that the results match exactly in the leading order of the perturbation.

We introduce the column matrices  $X$ ,  $V$  and a function  $Q(x, y)$  as follows,

$$X = \begin{pmatrix} x \\ y \end{pmatrix}, \quad V(x, y) = \begin{pmatrix} x^3 \\ 3x^2y \end{pmatrix}, \quad Q(x, y) = 1 - ax^2 - by^2. \quad (16)$$

The Eq. (8) can be expressed in a compact form,

$$\ddot{X} + (I + \beta\sigma_1)X + 2\Gamma\sigma_3Q(x, y)\dot{X} + \alpha V(x, y) = 0 \quad (17)$$

where  $\sigma_a, a = 1, 2, 3$  are the Pauli matrices. The perturbation analysis can be implemented in various ways by identifying one or more small parameters depending on the physical situations. As discussed in Ref. [12] and apparent from linear stability analysis, the periodic solutions are obtained for small gain-loss parameter  $\Gamma$ . Either the parameter  $\beta$  or  $\alpha$  or both of them can be chosen to be small parameters in order to implement perturbation scheme. In this article, we consider  $\Gamma$ ,  $\beta$  and  $\alpha$  as small parameters by choosing  $\Gamma = \epsilon\Gamma_0, \alpha = \epsilon\alpha_0, \beta = \epsilon\beta_0$ , where the parameter  $\epsilon$  is taken to be small, i.e.  $\epsilon \ll 1$ . The Eqn. (17) can be expressed as,

$$\ddot{X} + X + \epsilon \left[ 2\Gamma_0\sigma_3Q(x, y)\dot{X} + \beta_0\sigma_1X + \alpha_0\tilde{V}(x) \right] = 0. \quad (18)$$

The coordinates are expressed in powers of the small parameter  $\epsilon$

$$X = \sum_{n=0}^{\infty} \epsilon^n X^{(n)}, \quad X^{(n)} \equiv \begin{pmatrix} x_n \\ y_n \end{pmatrix}. \quad (19)$$

The equations at different orders of the small parameter  $\epsilon$  are obtained by substituting Eq. (19) in Eq. (18) and equating the terms with the same coefficient  $\epsilon^n$  to zero. The equations at the zeroth and the first orders are determined as,

$$\mathcal{O}(\epsilon^0) : \frac{d^2 X^{(0)}}{dt^2} + X^{(0)} = 0, \quad (20)$$

$$\mathcal{O}(\epsilon) : \frac{d^2 X^{(1)}}{dt^2} + X^{(1)} = -2\Gamma_0\sigma_3Q_0 \frac{dX^{(0)}}{dt} - \beta_0\sigma_1X^{(0)} - \alpha_0 \begin{pmatrix} x_0^3 \\ 3x_0^2y_0 \end{pmatrix}, \quad (21)$$

where we have defined  $Q_0 \equiv Q(x_0, y_0) = 1 - ax_0^2 - bx_0^2$ . The unperturbed solution of Eq. (20) has the form,

$$X^{(0)} = \mathcal{A} \exp(it) + c.c. \quad (22)$$

where c.c. denotes complex conjugate and the transpose of the constant column matrix  $\mathcal{A}$  is denoted as  $\mathcal{A}^T \equiv (A, B)$ . The solution  $X^{(0)}$  of the zeroth order equation is substituted in Eq. (21) resulting in the following inhomogeneous equation,

$$\begin{aligned} & \frac{d^2 X^{(1)}}{dt^2} + X^{(1)} = D \\ & D \equiv -e^{it} \left[ \beta_0\sigma_1\mathcal{A} + 2i\Gamma_0\sigma_3 \begin{pmatrix} A(1 - a|A|^2 - 2b|B|^2) + bB^2A^* \\ B(1 - b|B|^2 - 2a|A|^2) + aA^2B^* \end{pmatrix} \right. \\ & \left. + 3\alpha_0\mathcal{A} \begin{pmatrix} |A|^2 \\ AB^* + 2A^*B \end{pmatrix} \right] + e^{3it} \begin{pmatrix} -\alpha_0A^3 + 2i\Gamma_0A(aA^2 + bB^2) \\ -3\alpha_0A^2B - 2i\Gamma_0B(aA^2 + bB^2) \end{pmatrix} + c.c. \end{aligned} \quad (23)$$

The general solution up to the first order in  $\epsilon$  is obtained as,

$$X = \mathcal{A}e^{it} + \frac{i\epsilon t}{2}e^{it} \left[ \beta_0\sigma_1\mathcal{A} + 2i\Gamma_0\sigma_3 \begin{pmatrix} A(1 - a|A|^2 - 2b|B|^2) + bB^2A^* \\ B(1 - b|B|^2 - 2a|A|^2) + aA^2B^* \end{pmatrix} \right]$$



$$+ 3\alpha_0 \left( \begin{array}{c} |A|^2 A \\ A^2 B^* + 2|A|^2 B \end{array} \right) \Big] + \frac{\epsilon e^{3it}}{8} \left( \begin{array}{c} \alpha_0 A^3 - 2i\Gamma_0 A (aA^2 + bB^2) \\ 3\alpha_0 A^2 B + 2i\Gamma_0 B (aA^2 + bB^2) \end{array} \right) + c.c. + \mathcal{O}(\epsilon^2) \quad (24)$$

Note the appearance of secular terms which make the series divergent for large  $t > \frac{1}{\epsilon}$ . There are different regularization schemes. The Poincaré-Lindstedt method is not suitable for systems having multiple time-scales. We use the MSA method[34] in the next section. We employ RG method[35] in Sec. 2.2.2 to regularize the system and show that the results from both the methods agree at the first order of perturbation.

### 2.2.1 Method of multiple time-scales

We solve Eq. (18) perturbatively by using MSA methods. The unperturbed part of the system is described by two decoupled harmonic oscillators satisfying the equation  $\ddot{X} + X = 0$ . The terms with the coefficient  $\epsilon$  in Eq.(18) is treated as perturbation, which contain the effect of the loss-gain, coupling and nonlinear terms. The coordinates are expressed in powers of the small parameter  $\epsilon$  and multiple time-scales are introduced as follows,

$$T_n = \epsilon^n t, \quad X = \sum_{n=0}^{\infty} \epsilon^n X^{(n)}(T_0, T_1, \dots). \quad (25)$$

Substituting Eq.(25) in Eq.(18) and equating the terms with the same coefficient  $\epsilon^n$  to zero, the following equations up to  $\mathcal{O}(\epsilon)$  are obtained,

$$\mathcal{O}(\epsilon^0) : \quad \frac{\partial^2 X^{(0)}}{\partial T_0^2} + X^{(0)} = 0, \quad (26)$$

$$\mathcal{O}(\epsilon) : \quad \frac{\partial^2 X^{(1)}}{\partial T_0^2} + X^{(1)} = - \left[ 2 \frac{\partial^2 X^{(0)}}{\partial T_0 \partial T_1} + 2\Gamma_0 \sigma_3 Q_0 \frac{\partial X^{(0)}}{\partial T_0} + \beta_0 \sigma_1 X^{(0)} + \alpha_0 \left( \begin{array}{c} x_0^3 \\ 3x_0^2 y_0 \end{array} \right) \right] \quad (27)$$

These equations are to be solved consistently to get the perturbative results. Eq.(26) is solved as,

$$X^{(0)} = \left( \begin{array}{c} A(T_1, T_2, \dots) \\ B(T_1, T_2, \dots) \end{array} \right) \exp(iT_0) + c.c. \quad (28)$$

The integration constants  $A(T_1, T_2, \dots)$  and  $B(T_1, T_2, \dots)$  are independent of  $T_0$  and depend on slower time-scales. Eq. (27) is inhomogeneous, since the right hand side is independent of  $X^{(1)}$ . We define a column matrix  $\mathcal{B}$ ,

$$\begin{aligned} \mathcal{B} &= -e^{iT_0} \left[ 2i \frac{\partial \mathcal{A}}{\partial T_1} + \beta_0 \sigma_1 \mathcal{A} + 2i\Gamma_0 \sigma_3 \left( \begin{array}{c} A(1 - a|A|^2 - 2b|B|^2) + bB^2 A^* \\ B(1 - b|B|^2 - 2a|A|^2) + aA^2 B^* \end{array} \right) \right. \\ &\quad \left. + 3\alpha_0 A \left( \begin{array}{c} |A|^2 \\ AB^* + 2A^* B \end{array} \right) \right] + e^{3iT_0} \left( \begin{array}{c} -\alpha_0 A^3 + 2i\Gamma_0 A (aA^2 + bB^2) \\ -3\alpha_0 A^2 B - 2i\Gamma_0 B (aA^2 + bB^2) \end{array} \right) + c.c. \quad (29) \end{aligned}$$

Substituting Eq.(28) in Eq.(27), we obtain  $\frac{\partial^2 X^{(1)}}{\partial T_0^2} + X^{(1)} = \mathcal{B}$ . The term with the factors  $e^{\pm iT_0}$  in  $\mathcal{B}$  produce secular terms in  $X^{(1)}$  which must be eliminated for a uniform expansion. This is accomplished by setting the coefficients of  $e^{\pm iT_0}$  equal to zero:

$$2i \frac{\partial \mathcal{A}}{\partial T_1} + \beta_0 \sigma_1 \mathcal{A} + 2i\Gamma_0 \sigma_3 \left( \begin{array}{c} A(1 - a|A|^2 - 2b|B|^2) + bB^2 A^* \\ B(1 - b|B|^2 - 2a|A|^2) + aA^2 B^* \end{array} \right) + 3\alpha_0 A \left( \begin{array}{c} |A|^2 \\ AB^* + 2A^* B \end{array} \right) = 0. \quad (30)$$

The above equation governing the slow variation of the amplitudes results in a dimer model with the loss-gain terms depending linearly as well as nonlinearly on the dependent variables. The two modes of the dimer are coupled via loss-gain terms in addition to coupling through interaction terms. The VdPD oscillator in Eq. (8) reduces to the coupled Duffing oscillator system[12] with balanced loss and gain for  $a = b = 0$ . The dimer model corresponding to the Duffing oscillator system[12] is reproduced from Eq. (30) for  $a = b = 0$ , which has been shown to be exactly solvable admitting regular periodic solutions.

We introduce the Stokes variables as follows,

$$Z_a = 2\mathcal{A}^\dagger \sigma_a \mathcal{A}, \quad R = 2\mathcal{A}^\dagger \mathcal{A} = \sqrt{Z_1^2 + Z_2^2 + Z_3^2}, \quad (31)$$

which reduces Eq. (30) into four equations in terms  $Z_a$  and  $R$ :

$$\begin{aligned} \frac{\partial Z_1}{\partial T_1} &= 0, \quad Z_1(0) \equiv C_1 \\ \frac{\partial Z_2}{\partial T_1} &= \left( \beta_0 + \frac{3\alpha C_1}{4} \right) Z_3 + \frac{3\alpha_0 C_1}{4} R + \frac{\Gamma_0 Z_2}{2} [(b-a)R - (a+b)Z_3] \\ \frac{\partial Z_3}{\partial T_1} &= \frac{\Gamma_0}{2} [(a+b)Z_2^2 - R(4 - R(a+b) + Z_3(b-a))] - \left( \beta_0 + \frac{3\alpha_0 C_1}{4} \right) Z_2 \\ \frac{\partial R}{\partial T_1} &= \frac{\Gamma_0}{2} [(b-a)Z_2^2 - Z_3(4 - R(a+b) + Z_3(a-b))] + \frac{3\alpha_0}{4} C_1 Z_2 \end{aligned} \quad (32)$$

The quantity  $Z_1$  is a constant of motion and its value at  $t = 0$  is denoted as the constant  $C_1$ . It seems that the system of coupled nonlinear equations defined by Eq. (32) is not amenable to analytical solutions in its full generality. The linear stability analysis around the equilibrium point  $Z_2 = Z_3 = R = 0$  gives a set of coupled linear equations which have the form given by Eq. (32) with  $a = b = 0$ . It may be noted that Eq. (32) is exactly solvable in the limit  $a = b = 0$  and has been studied earlier in the context of coupled Duffing-oscillators system with BLG[12]. The general solution of Eq. (32) for small fluctuations around the equilibrium point may be obtained from Ref. [12] and one particular solution is reproduced<sup>1</sup> below for the sake of completeness:

$$\begin{aligned} A(t) &= \sqrt{\frac{C_1 \beta_0}{\eta}} e^{i \frac{2\eta^2 + 3C_1 \beta_0}{4\eta} \epsilon t}, \\ B(t) &= \sqrt{\frac{C_1}{2\eta} (2\beta_0 + 3\alpha C_1)} e^{i \left[ \frac{2\eta^2 + 3C_1 \beta_0}{4\eta} - \tan^{-1} \left( \frac{2\Gamma_0}{\eta} \right) \right] \epsilon t}. \end{aligned} \quad (33)$$

The stationary modes are obtained in regions of the parameter-space determined by the condition:

$$\begin{aligned} \eta^2 &\equiv \beta_0^2 + \frac{3}{2} \alpha \beta_0 C_1 - 4\Gamma_0^2 \geq 0, \\ \text{For } \alpha \geq 0 : C_1 \beta_0 &> 0, \quad \text{For } \alpha < 0 : 0 < C_1 \beta_0 < \frac{2\beta_0^2}{3|\alpha|} \end{aligned} \quad (34)$$

The expressions for  $(A, B)$  in Eq. (33) along with the condition (34) define approximate slow variation of the amplitudes to the leading order in the perturbation.

It appears that Eq. (30) is not analytically solvable with its full generality. The effect of space-dependence of the BLG terms is not seen in the approximate expressions (33) obtained

<sup>1</sup>The corresponding solution in Ref. [12] contains  $\epsilon^2 t$  instead of  $\epsilon t$  as in Eq. (33). This is because  $T_1 = \epsilon^2 t$  in Ref. [12], while  $T_1 = \epsilon t$  in the present article.

by linearizing the dimer system (32) which do not contain the parameters  $a, b$ . We find exact solutions of Eq. (30) for  $a \neq 0 \neq b$  with specific initial conditions and the effects of space-dependent BLG terms can be observed. We use polar decomposition of  $\mathcal{A}$ ,

$$A = A_0(T_1, T_2, \dots) e^{i\theta_A(T_1, T_2, \dots)}, B = B_0(T_1, T_2, \dots) e^{i\theta_B(T_1, T_2, \dots)}. \quad (35)$$

where the radial variables  $A_0, B_0$  and the phases  $\theta_A, \theta_B$  depend on slower time scales. The following equations are obtained after separating the real and imaginary parts of Eq. (30),

$$\begin{aligned} \frac{\partial A_0}{\partial T_1} + \Gamma_0 A_0 [1 - aA_0^2 - 2bB_0^2 + bB_0^2 \cos(2(\theta_B - \theta_A))] + \frac{1}{2} \sin(\theta_B - \theta_A) \beta_0 B_0 &= 0, \\ \frac{\partial B_0}{\partial T_1} - \Gamma_0 B_0 [1 - 2aA_0^2 - bB_0^2 + aA_0^2 \cos(2(\theta_B - \theta_A))] - \frac{1}{2} \sin(\theta_B - \theta_A) \beta_0 A_0 \\ + \frac{3\alpha_0}{2} B_0 A_0^2 \sin(2(\theta_A - \theta_B)) &= 0, \\ \frac{\partial \theta_B}{\partial T_1} - \frac{3\alpha_0}{2} A_0^2 [2 + \cos(2(\theta_B - \theta_A))] - \frac{\beta_0 A_0}{2B_0} \cos(\theta_B - \theta_A) + \Gamma_0 a A_0^2 \sin(2(\theta_B - \theta_A)) &= 0, \\ \frac{\partial \theta_A}{\partial T_1} + \frac{3\alpha_0}{2} A_0^2 - \frac{\beta_0 B_0}{2A_0} \cos(\theta_B - \theta_A) + \Gamma_0 b B_0^2 \sin(2(\theta_B - \theta_A)) &= 0. \end{aligned} \quad (36)$$

We take the limit of small  $\theta_A, \theta_B$  in the above equations and obtain,

$$\frac{\partial A_0}{\partial t} = -\Gamma A_0 [1 - (aA_0^2 + bB_0^2)], \quad (37)$$

$$\frac{\partial B_0}{\partial t} = \Gamma B_0 [1 - (aA_0^2 + bB_0^2)] \quad (38)$$

$$\frac{\partial \theta_A}{\partial t} = \frac{\beta B_0}{2A_0} - \frac{3\alpha A_0^2}{2}, \quad \frac{\partial \theta_B}{\partial t} = \frac{\beta A_0}{2B_0} + \frac{9\alpha A_0^2}{2} \quad (39)$$

which are exactly solvable. The limit of small  $\theta_A, \theta_B$  is equivalent to choosing the initial conditions  $X(0) = \mathcal{A}$  and  $\dot{X}(0) = 0$ . This leads the conditions on the zeroth order solutions  $X^{(0)}(0) = \mathcal{A}, \dot{X}^{(0)}(0) = 0$  and  $\theta_A^{(0)} = 0 = \theta_B^{(0)} \forall t$ . The phases  $\theta_A, \theta_B$  receive non-vanishing contribution only at the  $\mathcal{O}(\epsilon)$  and higher orders. The simplest case  $a = b = 0$  corresponds to coupled Duffing oscillators model of Ref. [12] and there are no periodic solutions for small  $\theta_A, \theta_B$  or equivalently with the initial conditions  $X^{(0)}(0) = \mathcal{A}, \dot{X}^{(0)}(0) = 0$ . The amplitude  $A_0$  decays with time for  $\Gamma > 0$  and becomes unbounded for  $\Gamma < 0$ . Similarly, the amplitude  $B_0$  grows exponentially with time for  $\Gamma > 0$  and decays for  $\Gamma < 0$ . The periodic solutions are obtained with different initial conditions[12]. However, periodic solutions are obtained in this limit for  $a \neq 0 \neq b$ . The effect of the space-dependent loss-gain terms is to change the nature of the solutions. Multiplying Eq. (37) by  $B_0$ , Eq. (38) by  $A_0$  and adding the resulting equations determine  $B_0 = \frac{K}{A_0}$ , where  $K$  is an integration constant. Substituting  $B$  in Eqs. (37,39) and denoting  $p = A_0^2$ , we obtain the following equations:

$$\frac{\partial p}{\partial t} = 2\Gamma (ap^2 - p + bK^2) \quad (40)$$

$$\theta_A = \int dt \left[ \frac{\beta K}{2p} + \frac{3\alpha}{2} p \right] + \theta_{A0}, \quad \theta_B = \int dt \left( \frac{\beta}{2K} + \frac{9\alpha}{2} \right) p + \theta_{B0}, \quad (41)$$

where  $\theta_{A0}$  and  $\theta_{B0}$  are integration constants. The primary task is to find the solution for  $p$  so that  $B_0 = \pm \frac{K}{\sqrt{p}}$  is determined directly and  $\theta_A, \theta_B$  are obtained after performing the integration.

For  $\Gamma = 0$ ,  $p$  is constant and  $\theta_A, \theta_B$  vary linearly with  $t$ . We consider  $\Gamma \neq 0$  for which Eq. (40) has three distinct solutions in three regions of parameter-space characterized by  $\Delta \equiv 1 - 4abK^2$ , where  $\Delta$  is the discriminant of the quadratic polynomial  $ap^2 - p + bK^2$ . The solution for  $\Delta < 0$  is singular at finite time and discarded. However, the solutions for  $\Delta = 0$  and  $\Delta > 0$  can be chosen to be finite for all time  $t \geq 0$  with appropriate choice of initial conditions. The solutions for  $A_0, B_0, \theta_A, \theta_B$  in these two regions for  $\Gamma \neq 0$  are described below.

The solution for  $\Delta = 0$ , *i.e.*  $K = \frac{1}{2\sqrt{ab}}$  has the form,

$$\begin{aligned} A_0(t) &= \sqrt{\frac{1}{2a}} \left(1 - \frac{1}{\Gamma t + c_1}\right)^{\frac{1}{2}}, \quad B_0(t) = \sqrt{\frac{1}{2b}} \left(1 - \frac{1}{\Gamma t + c_1}\right)^{-\frac{1}{2}}, \\ \theta_A(t) &= \left(\frac{\beta}{2}\sqrt{\frac{a}{b}} + \frac{3\alpha}{4a}\right)t + \frac{1}{\Gamma} \ln \left[ \frac{(\Gamma t + c_1 - 1)^{\frac{\beta}{2}\sqrt{\frac{a}{b}}}}{(\Gamma t + c_1)^{\frac{3\alpha}{4a}}} \right] + \frac{\beta(c_1 - 1)}{2\Gamma} \sqrt{\frac{a}{b}} + \theta_{A0} \\ \theta_B(t) &= \left(\frac{\beta}{2}\sqrt{\frac{b}{a}} + \frac{9\alpha}{4a}\right) \left(t - \frac{1}{\Gamma} \ln(\Gamma t + c_1)\right) + \theta_{B0} \end{aligned} \quad (42)$$

where  $c_1$  is an integration constant and we have chosen a positive  $K$  without loss of any generality. The factor  $\sqrt{\frac{a}{b}}$  is real either for  $(a, b) > 0$  or  $(a, b) < 0$ . We choose  $c_1 > 1$  for  $\Gamma > 0$  so that singularity at finite  $t$  within the range  $0 \leq t < \infty$  is avoided and  $A_0, B_0$  are real. We choose  $c_1 < 0$  for  $\Gamma < 0$  and the imaginary terms appearing in  $\theta_A$  and  $\theta_B$  from the negative of the logarithm may be absorbed in the integration constants  $\theta_{A0}$  and  $\theta_{B0}$ , respectively. Alternatively, the parameters may be chosen such that the quantities within the logarithm are always positive. The solution for  $\Delta > 0$ ,

$$\begin{aligned} A_0(t) &= \sqrt{\frac{1}{2a}} \left[1 - \frac{\sqrt{\Delta}}{2} \coth\left(\frac{\sqrt{\Delta}}{2}(\Gamma t + c_2)\right)\right]^{\frac{1}{2}}, \quad B_0(t) = \frac{K\sqrt{2a}}{\left[1 - \frac{\sqrt{\Delta}}{2} \coth\left(\frac{\sqrt{\Delta}}{2}(\Gamma t + c_2)\right)\right]^{\frac{1}{2}}} \\ \theta_A(t) &= \left(3\alpha + \frac{\beta}{4bK}\right)t + \frac{\beta c_2}{4bK\Gamma} + \left(\frac{\beta}{4bK} - 3\alpha\right) \frac{1}{\Gamma} \ln \left\{ \sinh\left(\frac{\sqrt{\Delta}}{2}(\Gamma t + c_2)\right) \right\} \\ &\quad + \frac{\beta}{4bK\Gamma} \ln \left\{ 2 \coth\left(\frac{\sqrt{\Delta}}{2}(\Gamma t + c_2)\right) - \sqrt{\Delta} \right\} + \theta_{A0} \\ \theta_B(t) &= \frac{1}{4a} \left(\frac{\beta}{K} + 9\alpha\right) \left[t - \frac{1}{\Gamma} \ln \left\{ \sinh\left(\frac{\sqrt{\Delta}}{2}(\Gamma t + c_2)\right) \right\}\right] + \theta_{B0} \end{aligned} \quad (43)$$

where the integration constant  $c_2$  satisfies the condition  $\coth^{-1}\left(\frac{\sqrt{\Delta}}{2}\right) < c_2 < \coth^{-1}\left(\frac{2}{\sqrt{\Delta}}\right)$  for  $\Gamma > 0$  which implies  $\Delta > 4$ . The condition  $\Delta > 4$  can be implemented in various ways: (i)  $a > 0, b > 0, K < 0$ , (ii)  $a < 0, b < 0, K < 0$ , (iii)  $a > 0, b < 0, K > 0$ , (iv)  $a < 0, b > 0, K > 0$ . We choose the cases (i) and (iii) so that  $A_0$  and  $B_0$  are real. The constant  $c_2$  may be chosen as  $c_2 < 0$  for  $\Gamma < 0$  and the imaginary terms appearing in  $\theta_A$  and  $\theta_B$  from the negative of the logarithm may be absorbed in the integration constants  $\theta_{A0}$  and  $\theta_{B0}$ , respectively. Alternatively, the parameters may be chosen such that the quantities within the the logarithm are always positive. The constants  $\theta_{A0}$  and  $\theta_{B0}$  may be chosen appropriately for both  $\Delta = 0$  and  $\Delta > 0$  so that  $\theta_A(0) = 0 = \theta_B(0)$ . The integration constants  $c_1$  and  $c_2$  may be chosen appropriately to fix the values of  $A_0(0)$  and  $B_0(0)$  depending on the physical requirement.

### 2.2.2 RG Techniques

The RG technique involves introducing an intermediate time  $\tau$  within the time-interval  $(t_0, t)$  to split it into two sub-intervals as  $t - t_0 = (t - \tau) + (\tau - t_0)$ , where the initial time  $t_0 = 0$  for the present case. The objective is to cancel the secular terms at the moment  $\tau$  and construct the slow time-dependence of the integration constant  $\mathcal{A}$  of the unperturbed problem. We denote  $\mathcal{A} = \mathcal{A}(0)$  to distinguish it from the amplitude  $\mathcal{A}(t)$  where slow time-variation has been incorporated. The  $\mathcal{A}(0)$  is expanded as follows,

$$\mathcal{A}(0) = \mathcal{A}(\tau) + \sum_{n=1}^{\infty} \epsilon^n \mathcal{A}^T(\tau) \mathcal{A}^{(n)}, \quad \mathcal{A}^{(n)} \equiv \begin{pmatrix} a^{(n)} \\ b^{(n)} \end{pmatrix} \quad (44)$$

where  $a^{(n)}, b^{(n)}$  are constants. We rewrite the overall multiplicative factor  $t$  in the second term of Eq. (24) as  $t = (t - \tau) + \tau$ , substitute the expressions for  $\mathcal{A}(0)$  by using Eq. (44) and keep the terms up to the order of  $\epsilon$ . The coefficients  $a^{(1)}, b^{(1)}$  are chosen such that the terms proportional to  $\tau$  are cancelled by keeping the terms proportional to  $t - \tau$ :

$$\mathcal{A}^{(1)} = -\frac{i\tau}{2} \left[ \beta_0 \sigma_1 \mathcal{A} + 2i\Gamma_0 \sigma_3 \begin{pmatrix} A(1 - a|A|^2 - 2b|B|^2) + bB^2 A^* \\ B(1 - b|B|^2 - 2a|A|^2) + aA^2 B^* \end{pmatrix} + 3\alpha_0 \begin{pmatrix} |A|^2 A \\ A^2 B^* + 2|A|^2 B \end{pmatrix} \right] \quad (45)$$

The resulting expression for  $X$  depends on  $\tau$  explicitly:

$$\begin{aligned} X &= e^{it} \left[ \mathcal{A} + \frac{i\epsilon(t - \tau)}{2} \left\{ \beta_0 \sigma_1 \mathcal{A} + 2i\Gamma_0 \sigma_3 \begin{pmatrix} A(1 - a|A|^2 - 2b|B|^2) + bB^2 A^* \\ B(1 - b|B|^2 - 2a|A|^2) + aA^2 B^* \end{pmatrix} \right. \right. \\ &\quad \left. \left. + 3\alpha_0 \begin{pmatrix} |A|^2 A \\ A^2 B^* + 2|A|^2 B \end{pmatrix} \right\} \right] + \frac{\epsilon e^{3it}}{8} \begin{pmatrix} \alpha_0 A^3 - 2i\Gamma_0 A (aA^2 + bB^2) \\ 3\alpha_0 A^2 B + 2i\Gamma_0 B (aA^2 + bB^2) \end{pmatrix} + c.c. + \mathcal{O}(\epsilon^2) \end{aligned}$$

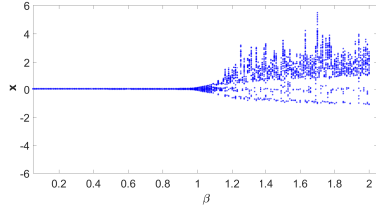
The parameter  $\tau$  does not appear in the original problem and should not be present in the final solution. The  $\tau$ -dependence of  $X$  is removed by imposing  $\frac{\partial X}{\partial \tau} \Big|_{\tau=t} = 0, \forall t$  leading to the RG flow equation which is same as Eq. (30) with the substitution of  $T_1 = \epsilon t, \alpha = \epsilon \alpha_0, \beta = \epsilon \beta_0, \Gamma = \epsilon \Gamma_0$ . The removal of  $\tau$  requires setting  $\tau = t$  for which the secular terms vanish and the expression of  $X$  is given as,

$$X = e^{it} \mathcal{A} + \frac{\epsilon e^{3it}}{8} \begin{pmatrix} \alpha_0 A^3 - 2i\Gamma_0 A (aA^2 + bB^2) \\ 3\alpha_0 A^2 B + 2i\Gamma_0 B (aA^2 + bB^2) \end{pmatrix} + c.c. + \mathcal{O}(\epsilon^2), \quad (46)$$

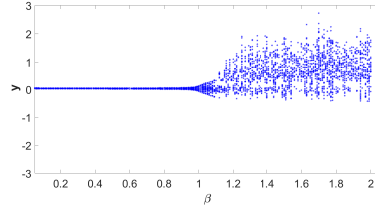
where the modulus and phases of  $A(t), B(t)$ , i.e.  $(A_0, \theta_A), (B_0, \theta_B)$  are given by Eq. (42) for  $\Delta = 0$  and from Eq. (43) for  $\Delta > 0$ .

### 2.3 Numerical Solution

The Hamiltonian system is described in terms of five independent parameters  $\Gamma, \beta, \alpha, a$  and  $b$ . We have numerically studied the bifurcation diagram by varying one of these parameters and keeping the remaining four parameters as fixed. The bifurcation diagrams for varying  $\beta$  is shown in Fig. 1 for  $\Gamma = 0.01$  and  $\alpha = 0.5$  with the initial values of the dynamical variables chosen around the point  $P_0$ . The time-series has different behaviours depending on the values of  $\beta$ . The regular periodic solutions are obtained in the range  $0 \leq \beta < 1.05$  and the chaotic behavior onsets from  $\beta \geq \beta_c = 1.05$ . The bifurcation diagram is symmetric with respect to the point  $\beta = 0$  and the results are shown only for  $\beta \geq 0$ . The qualitative feature of the bifurcation diagram is similar to the case with  $a = b = 0$ . The crossover from regular to chaotic dynamics as  $\beta$  is varied



(a)  $\alpha = 0.5, \Gamma = 0.01, a = 1.0, b = 1.0$



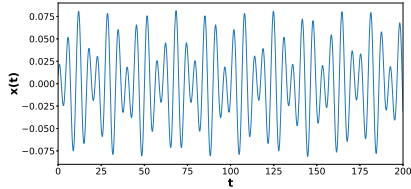
(b)  $\alpha = 0.5, \Gamma = 0.01, a = 1.0, b = 1.0$

Figure 1: (Color online) Bifurcation diagrams for  $\beta$  with the initial conditions  $x(0) = 0.01$ ,  $y(0) = 0.02$ ,  $\dot{x}(0) = 0.03$ ,  $\dot{y}(0) = 0.04$

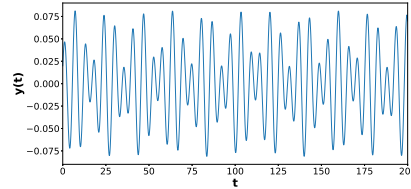
through  $\beta_c$  may be understood by interpreting the  $x$  degree of freedom as describing a forced VdPD oscillator with the identification of  $\beta y$  as the forcing term. Unlike the standard forced VdPD oscillator, the forcing is determined in a nontrivial way from the solution of the system. The chaotic behaviour of  $y$  degree of freedom is induced via its coupling to the  $x$  degree of freedom. The two oscillators are also coupled via the space-dependent loss-gain terms. However, the bifurcation diagram for varying  $b$  and constant  $\alpha, \beta, \Gamma, a$  does not show any chaotic behaviour under the similar initial conditions for  $\beta = 0$  as well as  $\beta \neq 0$ .

### 2.3.1 Regular Dynamics

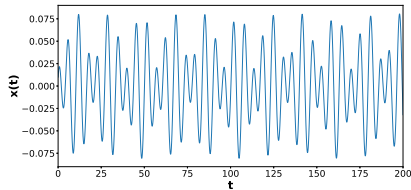
The time-series of the dynamical variables in the vicinity of the point  $P_0$  is shown in Fig. 2 for  $\Gamma = 0.2, \beta = 0.5, \alpha = 1.0, a = b$  and  $a \neq b$ . Periodic solutions in Figs. 2a and 2b correspond to  $a = 1.0, b = 1.0$ , while Figs. (2c) and (2d) correspond to  $a = 1.0, b = 5.0$ . It may be noted that



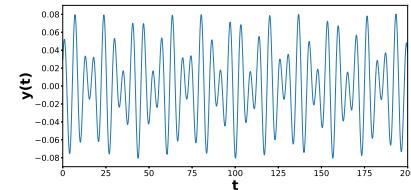
(a)  $\alpha = 1.0, \beta = 0.5, \Gamma = 0.2, a = 1.0, b = 1.0$



(b)  $\alpha = 1.0, \beta = 0.5, \Gamma = 0.2, a = 1.0, b = 1.0$



(c)  $\alpha = 1.0, \beta = 0.5, \Gamma = 0.2, a = 1.0, b = 5.0$

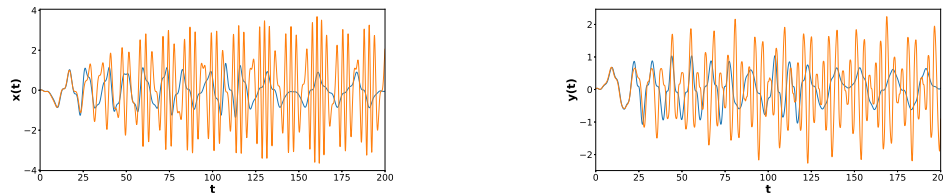


(d)  $\alpha = 1.0, \beta = 0.5, \Gamma = 0.2, a = 1.0, b = 5.0$

Figure 2: (Color online) Regular solutions of Eq. (8) in the vicinity of the point  $P_0$  with the initial conditions  $x(0) = 0.01, y(0) = 0.02, \dot{x}(0) = 0.03$  and  $\dot{y}(0) = 0.04$ .

the time evolution of the dynamical variables with the same initial conditions and fixed  $\Gamma, \beta, a, b$  show similar oscillatory behaviour for positive as well as negative  $\alpha$ . There are minute changes in amplitudes and phases and that too in the limit of large  $t$ . The Lyapunov exponents and the

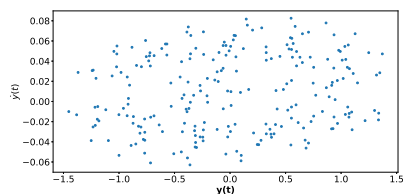
autocorrelation functions for the time series representing the periodic solutions in Fig. 2 have been calculated to confirm that these solutions are indeed regular. The numerical results are consistent with perturbative analysis.



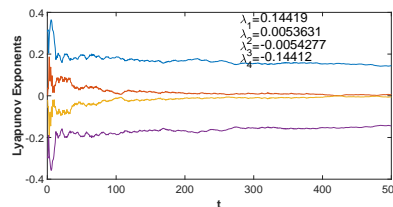
(a)  $\Gamma = 0.01, \beta = 1.3, \alpha = 0.5, a = 1.0, b = 1.0$

(b)  $\Gamma = 0.01, \beta = 1.3, \alpha = 0.5, a = 1.0, b = 1.0$

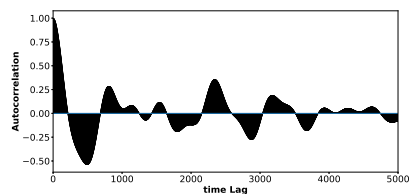
Figure 3: (Color online) Chaotic solutions of Eq. (8) with two sets of initial conditions (a)  $x(0) = 0.01, y(0) = 0.02, \dot{x}(0) = 0.03, \dot{y}(0) = 0.04$  (blue color) and (b)  $x(0) = 0.01, y(0) = 0.025, \dot{x}(0) = 0.03, \dot{y}(0) = 0.04$  (orange color).



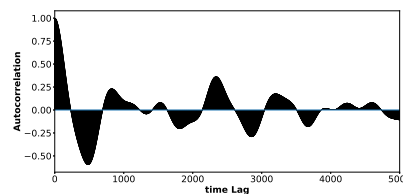
(a) Poincaré section:  $\dot{y}(t)$  VS.  $y(t)$  plot



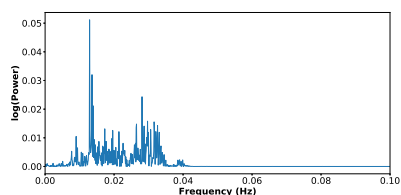
(b) Lyapunov exponents



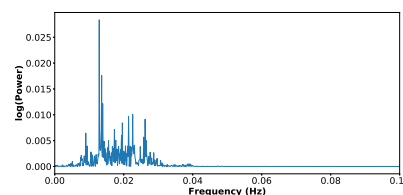
(c) Autocorrelation function of  $x(t)$



(d) Autocorrelation function of  $y(t)$



(e) Powerspectra of  $x(t)$



(f) Powerspectra of  $y(t)$

Figure 4: (Color online) Poincaré section, Lyapunov exponents, autocorrelation function and power spectra for  $\Gamma = 0.01, \beta = 1.3, \alpha = 0.5, a = 1.0, b = 1.0$  with the initial condition  $x(0) = 0.01, y(0) = 0.02, \dot{x}(0) = 0.03, \dot{y}(0) = 0.04$ . The plots corresponding to the largest ( $\lambda_1 = 0.14419$ ) and the smallest ( $\lambda_2 = -0.14412$ ) Lyapunov exponents are denoted by blue and violet colors, respectively.

### 2.3.2 Chaotic Dynamics

The bifurcation diagram is given in Fig. 1, where  $x$  and  $y$  are plotted as a function of  $\beta$  for fixed values of  $\alpha = 0.5, \Gamma = 0.01, a = 1.0, b = 1.0$ . It is seen that the system is chaotic for  $\beta > \beta_c = 1.05$ . The study of sensitivity of the dynamical variables to the initial conditions is one of the important methods to check whether the system is chaotic or not. The two sets of initial conditions: (a)  $x(0) = 0.01, y(0) = 0.02, \dot{x}(0) = 0.03, \dot{y}(0) = 0.04$  and (b)  $x(0) = 0.01, y(0) = 0.02, \dot{x}(0) = 0.03, \dot{y}(0) = 0.025$  are considered in order to study the sensitivity of the dynamical variables to the initial conditions in different regions of the parameters. It may be noted that these two initial conditions are identical except for the values of  $\dot{y}(0)$  which differ by 0.015. The Fig. 3 represents the time series of the dynamical variables in the chaotic regime for  $\beta = 1.3$ . A few other independent methods are also employed to confirm the chaotic behaviour in the model. In this regard, the auto-correlation function, Lyapunov exponent, Poincaré section and power spectra are plotted in Fig. 4. The Lyapunov exponents are computed up to seven decimal places (0.14419, 0.0063631,  $-0.0054277, -0.14412$ ). It is known that the sum of the Lyapunov exponents are zero for a Hamiltonian system, which is valid for the present case if values up to the 2nd decimal places are considered with an error of the order of  $10^{-3}$ .

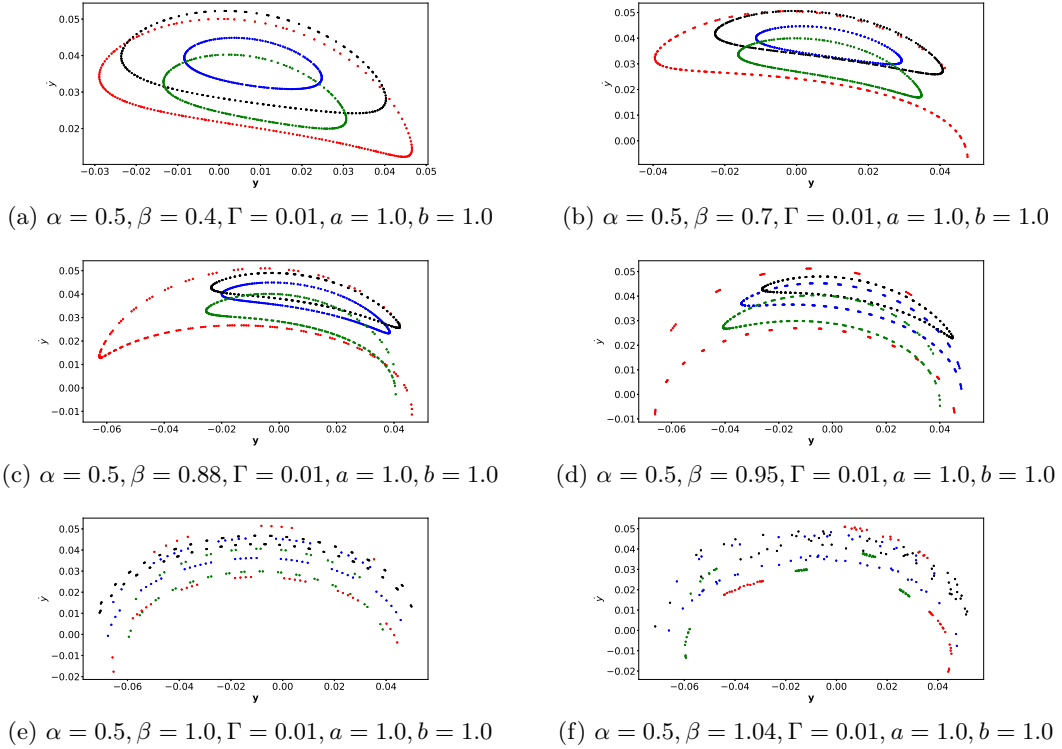


Figure 5: (Color online) Poincaré sections of Eq. (8) with four sets of initial conditions: (a)  $x(0) = 0.01, y(0) = 0.02, \dot{x}(0) = 0.03, \dot{y}(0) = 0.04$  (blue color), (b)  $x(0) = 0.01, y(0) = 0.03, \dot{x}(0) = 0.015, \dot{y}(0) = 0.04$  (red color), (c)  $x(0) = 0.01, y(0) = 0.04, \dot{x}(0) = 0.025, \dot{y}(0) = 0.03$  (black color) and (d)  $x(0) = 0.01, y(0) = 0.025, \dot{x}(0) = 0.03, \dot{y}(0) = 0.02$  (green color)

The route to chaos may be studied in terms of the qualitative changes in a set of Poincaré sections of the system as the parameter  $\beta$  is varied from the non-chaotic to the chaotic region.



The set of Poincaré sections corresponds to independent initial conditions  $(x(0), y(0), \dot{x}(0), \dot{y}(0))$  around the equilibrium point  $P_0$ . This effectively allows us to study the dynamics of the system on the chosen Poincaré sections. We consider four different initial conditions for a given  $\beta$  as follows: (i) (0.01, 0.02, 0.03, 0.04), (ii) (0.01, 0.03, 0.015, 0.04), (iii) (0.01, 0.04, 0.025, 0.03), and (iv) (0.01, 0.025, 0.03, 0.02). The corresponding surface of sections change differently for different values of  $\beta$ . It is seen from Fig. 5 that all four orbits on the chosen surface are closed for  $\beta = 0.5$ . The total number of closed orbits gradually reduce to 1 around  $\beta = 0.95$ , and finally no closed orbits are seen as the critical value  $\beta_c = 1.05$  is approached. The breaking of closed orbits on the surface of section correspond to breaking of tori in the original four dimensional state-velocity space. There are only isolated points in the chaotic region, i.e. beyond  $\beta > \beta_c$ .

### 3 Non- $\mathcal{PT}$ -symmetric non-Hamiltonian system

In this section, we consider a system by modifying the nonlinear interaction  $3gx^2y$  in Eq. (1) to  $\tilde{g}y^3$ . The equations of motion for the system in terms of the dimensionless variables introduced in Eqs. (6, 7) are,

$$\begin{aligned} \ddot{x} + 2\Gamma(1 - ax^2 - by^2)\dot{x} + x + \beta y + \alpha x^3 &= 0, \\ \ddot{y} - 2\Gamma(1 - ax^2 - by^2)\dot{y} + y + \beta x + \tilde{\alpha}y^3 &= 0, \end{aligned} \quad (47)$$

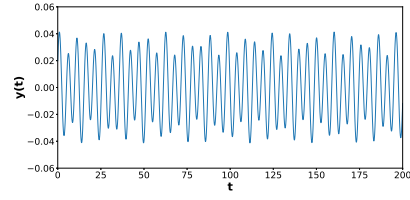
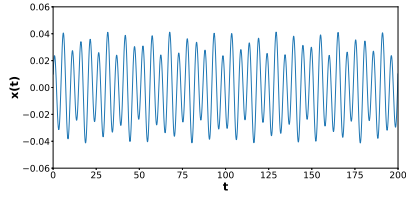
where we have chosen  $\text{sgn}(\beta_1) = \text{sgn}(\beta_2)$  for simplicity and  $\tilde{\alpha} = \frac{\tilde{g}}{|\beta_1|\omega^2}$ . The system described by Eq. (47) is a generalization of the models considered in Refs. [1, 33]. The model of [33] is obtained for  $\alpha = \tilde{\alpha}$ ,  $a = 0 = b$ , while the system described in Ref. [1] is obtained for  $a = 0 = b$  and without any constraint on  $\alpha, \tilde{\alpha}$ . The generalized system describes two coupled VdPD oscillators with balanced loss and gain. The  $x$ -degree of freedom describes the standard VdPD oscillator for  $\beta = 0 = b$ , while the  $y$  degree of freedom describes a damped Duffing oscillator with the linear restoring force depending on  $x$ . Similarly, for  $\beta = 0 = a$ , there is a role reversal for the  $x$  and  $y$  degrees of freedom. The space-dependence of the gain and loss terms should be identical so that the flow preserves the volume in the position-velocity state space[11]. We choose the space-dependence of the loss-gain terms as  $1 - ax^2 - by^2$  so that the forms  $1 - ax^2$  and  $1 - by^2$  may be considered for  $b = 0$  and  $a = 0$ , respectively. It is worth mentioning here that a similar system with additional velocity mediated coupling terms and unbalanced loss-gain terms, where the damping/anti-damping term varies linearly with space-coordinates, has been reported to admit amplitude death[40]. We consider a balanced loss-gain system which exhibits periodic solutions in the regular regime.

It stems from the linear stability analysis of the system that the coupling between the two systems via non-vanishing  $\beta$  is required for the existence of periodic solutions. The stability criteria for the systems defined by Eqs. (8) and (47) are identical. The system is  $\mathcal{PT}$ -symmetric for  $a = b$  and  $\alpha = \tilde{\alpha}$ , and non- $\mathcal{PT}$ -symmetric if any of these conditions are violated. It will be seen that the dynamical behaviour of the system is quite rich, including existence of periodic solutions, for the  $\mathcal{PT}$ -symmetric as well as non- $\mathcal{PT}$ -symmetric regime. The Hamiltonian for the system can not be constructed by using the techniques outlined in Ref. [8, 10] for  $\alpha \neq 0 \neq \tilde{\alpha}$ .

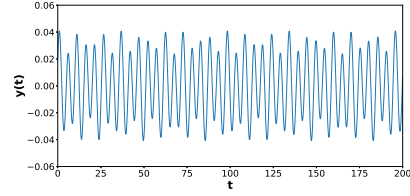
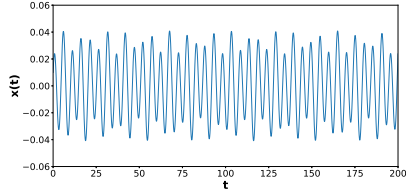
The MSA and the RG techniques can be carried forward in a straightforward way and the slow variation of the amplitude is governed by the equation,

$$2i\frac{\partial \mathcal{A}}{\partial T_1} + \beta_0\sigma_1\mathcal{A} + 2i\Gamma_0\sigma_3 \left( \frac{A(1 - a|A|^2 - 2b|B|^2) + bB^2A^*}{B(1 - b|B|^2 - 2a|A|^2) + aA^2B^*} \right) + 3\alpha_0 \left( \frac{|A|^2A}{|B|^2B} \right) = 0 \quad (48)$$

Note that Eq. (48) differs from the corresponding Eq. (30) for the Hamiltonian system in the last term. In the limit of small  $\theta_A, \theta_B$ , the amplitudes  $A_0, B_0$  and the phase  $\theta_A$  are determined

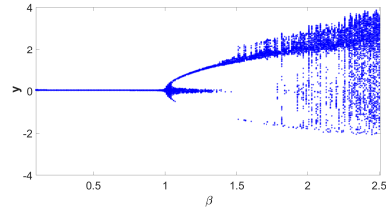
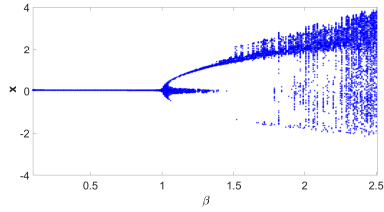


(a)  $\alpha = \tilde{\alpha} = 0.5, \beta = 0.5, \Gamma = 0.03, a = 1.0, b = 1.0$  (b)  $\alpha = \tilde{\alpha} = 0.5, \beta = 0.5, \Gamma = 0.03, a = 1.0, b = 1.0$



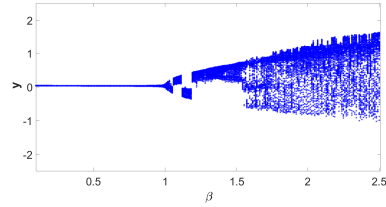
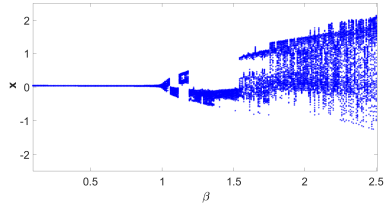
(c)  $\alpha = 1.0, \tilde{\alpha} = 3.0, \beta = 0.5, \Gamma = 0.01, a = 1.0, b = 2.0$  (d)  $\alpha = 1.0, \tilde{\alpha} = 3.0, \beta = 0.5, \Gamma = 0.01, a = 1.0, b = 2.0$

Figure 6: (Color online) Solutions of Eq.(47) in the vicinity of the point  $P_0$  with the initial conditions  $x(0) = 0.01, y(0) = 0.02, \dot{x}(0) = 0.03$  and  $\dot{y}(0) = 0.04$ . The results for  $\mathcal{PT}$ -symmetric and non- $\mathcal{PT}$ -symmetric regions are described in the first and the second rows, respectively.



(a)  $\alpha = \tilde{\alpha} = 0.5, \Gamma = 0.03, a = 1.0, b = 1.0$

(b)  $\alpha = \tilde{\alpha} = 0.5, \Gamma = 0.03, a = 1.0, b = 1.0$



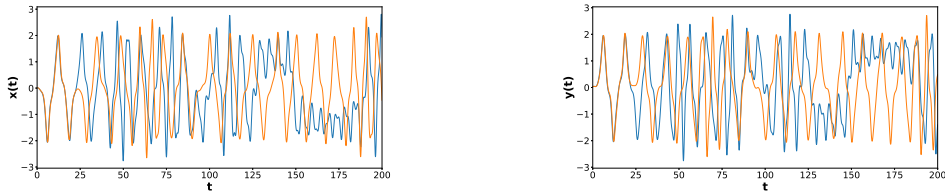
(c)  $\alpha = 1.0, \tilde{\alpha} = 3.0, \Gamma = 0.01, a = 1.0, b = 2.0$

(d)  $\alpha = 1.0, \tilde{\alpha} = 3.0, \Gamma = 0.01, a = 1.0, b = 2.0$

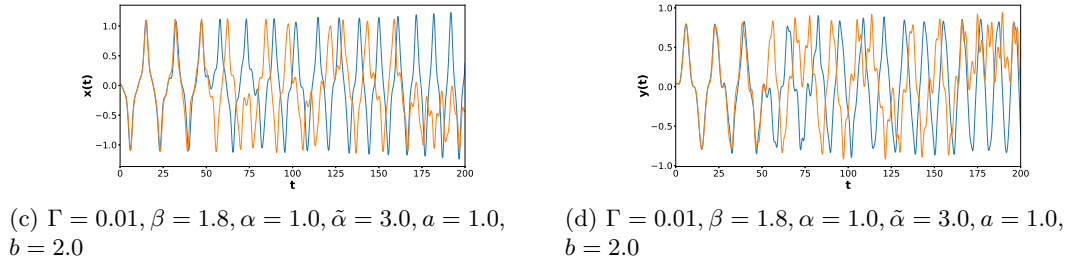
Figure 7: (Color online) Bifurcation diagrams of Eq. (47) in the vicinity of the point  $P_0$  with the initial conditions  $x(0) = 0.01, y(0) = 0.02, \dot{x}(0) = 0.03$  and  $\dot{y}(0) = 0.04$ . The results for the  $\mathcal{PT}$ -symmetric and non- $\mathcal{PT}$ -symmetric regions are given in the first and the second rows, respectively.

by the Eqs. (37, 38) and the first equation of (39). The equation for  $\theta_B$  is different and given by,

$$\frac{\partial \theta_B}{\partial t} = \frac{\beta A_0}{2B_0} + \frac{3\alpha B_0^2}{2} \Rightarrow \theta_B = \frac{\beta}{2K} p + \frac{3\alpha K}{2p} + \theta_{B0} \quad (49)$$



(a)  $\Gamma = 0.03, \beta = 2.0, \alpha = \tilde{\alpha} = 0.5, a = 1.0, b = 1.0$  (b)  $\Gamma = 0.03, \beta = 2.0, \alpha = \tilde{\alpha} = 0.5, a = 1.0, b = 1.0$



(c)  $\Gamma = 0.01, \beta = 1.8, \alpha = 1.0, \tilde{\alpha} = 3.0, a = 1.0, b = 2.0$  (d)  $\Gamma = 0.01, \beta = 1.8, \alpha = 1.0, \tilde{\alpha} = 3.0, a = 1.0, b = 2.0$

Figure 8: (Color online) Chaotic solutions of Eq. (47) with two sets of initial conditions (a)  $x(0) = 0.01, y(0) = 0.02, \dot{x}(0) = 0.03, \dot{y}(0) = 0.04$  (blue color) and (b)  $x(0) = 0.01, y(0) = 0.025, \dot{x}(0) = 0.03, \dot{y}(0) = 0.04$  (orange color). The first row describes results in the  $\mathcal{PT}$ -symmetric region, while the figures in the second row correspond to non- $\mathcal{PT}$ -symmetric regime.

where we have used  $B_0 = \frac{K}{A_0}$  in the last step. Thus, in the leading order of the perturbation, only  $\theta_B$  is different for the systems defined by Eqs. (8) and (47). The solution for  $p$  from Eqs (40) may be substituted to get the expression for  $\theta_B$ .

### 3.1 Numerical Solution

The system is analyzed by numerical analysis which reveals a rich complex dynamical behaviour. The regular dynamics admitting periodic solutions is consistent with perturbative analysis. The results of numerical investigations are presented in the  $\mathcal{PT}$ -symmetric regime ( $a = b, \alpha = \tilde{\alpha}$ ) as well as in the non- $\mathcal{PT}$ -symmetric regime ( $a \neq b, \alpha \neq \tilde{\alpha}$ ) for different values of  $\Gamma$  and  $\beta$  for which  $P_0$  is a center. We choose  $a = b = 1.0, \alpha = \tilde{\alpha} = 0.5$  for numerical results in the  $\mathcal{PT}$ -symmetric region. The results in the non- $\mathcal{PT}$ -symmetric region are presented with  $a = 1.0, b = 2.0, \alpha = 1.0, \tilde{\alpha} = 3.0$ . The values of  $\Gamma$  and  $\beta$  are chosen depending on the particular object of physical interest. The initial conditions for all the numerical investigations are chosen as  $x(0) = 0.01, y(0) = 0.02, \dot{x}(0) = 0.03$  and  $\dot{y}(0) = 0.04$ , unless specified otherwise, which correspond to small fluctuations around the equilibrium point  $P_0$ . The time-series of  $x$  and  $y$  in the  $\mathcal{PT}$ -symmetric regime is presented in the first row of Fig. 6 for  $\beta = 0.5, \Gamma = 0.03$ . The periodic solution in the non- $\mathcal{PT}$ -symmetric region for  $\Gamma = 0.01$  and  $\beta = 0.5$  is presented in the second row of Fig. 6. The periodic solution of non-Hamiltonian, non- $\mathcal{PT}$ -symmetric VdPD oscillator is yet another example where the existence of bounded solution is not attributed to unbroken  $\mathcal{PT}$ -symmetry. The bifurcation diagrams in Fig. 7 show that the system is chaotic for  $\beta > \beta_c$  both in the  $\mathcal{PT}$ -symmetric as well as non- $\mathcal{PT}$ -symmetric regimes. The value of  $\beta_c$  in the  $\mathcal{PT}$ -symmetric regime is 1.07, while it is 1.05 in the non- $\mathcal{PT}$ -symmetric region. The values of the parameters for these two cases are different and a direct comparison of the values of  $\beta_c$  is not going to give any information. The sensitivity of the dynamical variables to the initial conditions are studied in different regions of the parameter-space by considering two sets of initial conditions: (a)  $x(0) = 0.01, y(0) =$

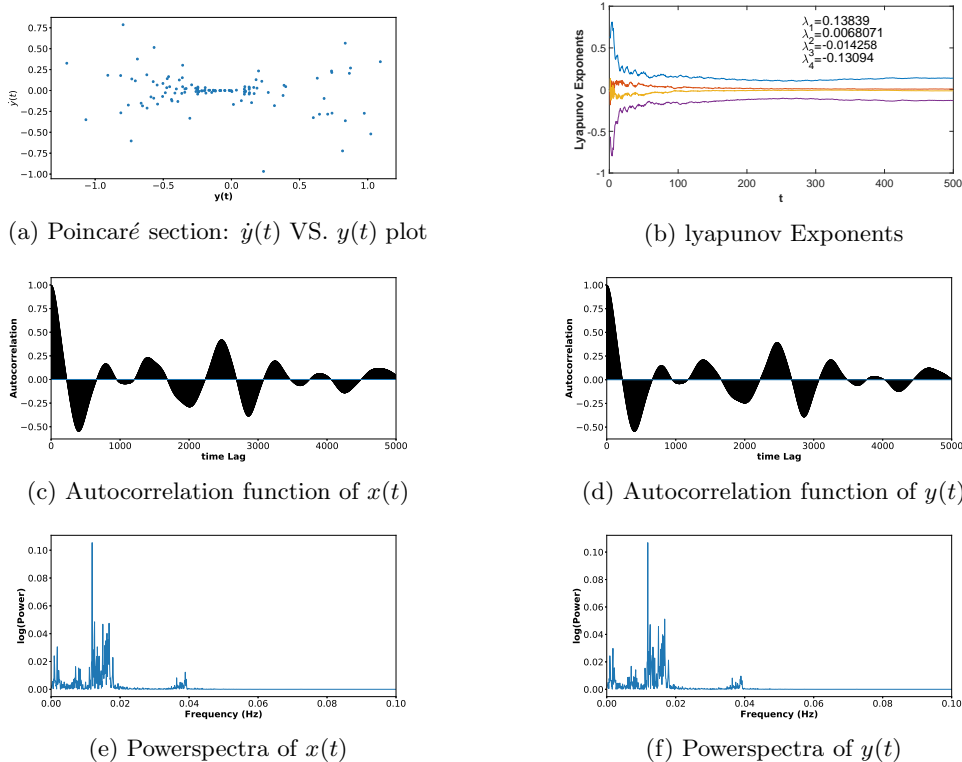
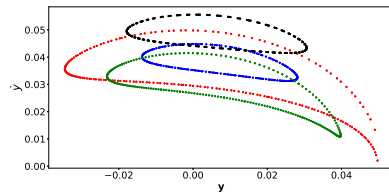
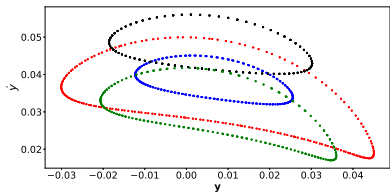


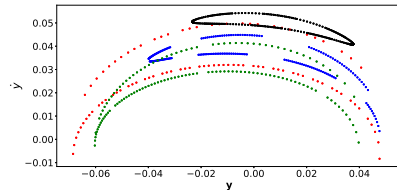
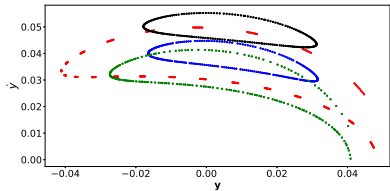
Figure 9: (Color online) Poincaré section, Lyapunov exponents, autocorrelation function and power spectra for  $\Gamma = 0.03, \beta = 2.0, \alpha = \tilde{\alpha} = 0.5, a = 1.0, b = 1.0$  with the initial conditions  $x(0) = 0.01, y(0) = 0.02, \dot{x}(0) = 0.03, \dot{y}(0) = 0.04$

$0.02, \dot{x}(0) = 0.03, \dot{y}(0) = 0.04$  and (b)  $x(0) = 0.01, y(0) = 0.02, \dot{x}(0) = 0.03, \dot{y}(0) = 0.025$ . These two initial conditions are identical except for the values of  $\dot{y}(0)$  which differ by  $0.015$ . The time series of the dynamical variables in the chaotic regime is presented in Fig. 8—the first row corresponds to  $\mathcal{PT}$ -symmetric region with  $\beta = 2.0, \Gamma = 0.03$  and the second-row for the non- $\mathcal{PT}$ -symmetric region for  $\beta = 1.8, \Gamma = 0.01$ . The chaotic behaviour in the model has been confirmed by other independent methods also. In this regard, the auto-correlation function, Lyapunov exponent, Poincaré section and power spectra are plotted in Figs. 9 and 11 for  $\mathcal{PT}$ -symmetric and non- $\mathcal{PT}$ -symmetric regimes, respectively. The Lyapunov exponents in the  $\mathcal{PT}$ -symmetric region is computed up to six decimal places ( $0.13839, 0.0068071, -0.014258, -0.13094$ ), while it is computed up to seven decimal places ( $0.041361, 0.0021885, -0.0061831, -0.037366$ ) for the non- $\mathcal{PT}$ -symmetric case.

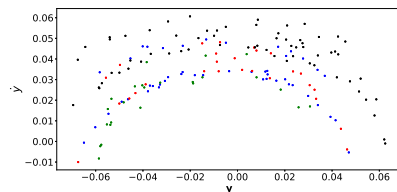
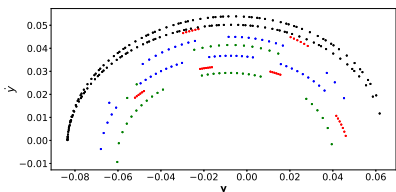
The route to chaos for the non-Hamiltonian system with or without  $\mathcal{PT}$ -symmetry may be studied in terms of the qualitative changes in a set of Poincaré sections of the system as the parameter  $\beta$  is varied from the non-chaotic to the chaotic region. The qualitative features are similar to that of the Hamiltonian system. It is seen from Fig. 10 corresponding to the  $\mathcal{PT}$ -symmetric non-Hamiltonian system that all four orbits on the chosen surface are closed for  $\beta = 0.65$  and only one orbit is closed around  $\beta = 0.97$ , and finally no closed orbits are seen as the critical value  $\beta_c = 1.05$  is approached. There are only isolated points in the chaotic region, i.e. beyond  $\beta > \beta_c$ . The scenario for non- $\mathcal{PT}$ -symmetric non-Hamiltonian system is similar to the



(a)  $\alpha = \tilde{\alpha} = 0.5, \beta = 0.65, \Gamma = 0.03, a = 1.0, b = 1.0$  (b)  $\alpha = \tilde{\alpha} = 0.5, \beta = 0.76, \Gamma = 0.03, a = 1.0, b = 1.0$



(c)  $\alpha = \tilde{\alpha} = 0.5, \beta = 0.85, \Gamma = 0.03, a = 1.0, b = 1.0$  (d)  $\alpha = \tilde{\alpha} = 0.5, \beta = 0.97, \Gamma = 0.03, a = 1.0, b = 1.0$



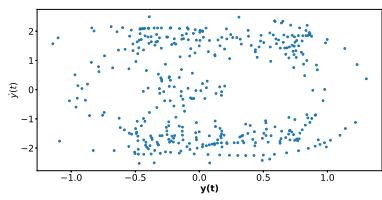
(e)  $\alpha = \tilde{\alpha} = 0.5, \beta = 1.0, \Gamma = 0.03, a = 1.0, b = 1.0$  (f)  $\alpha = \tilde{\alpha} = 0.5, \beta = 1.08, \Gamma = 0.03, a = 1.0, b = 1.0$

Figure 10: (Color online) Poincaré section of Eq. (47) with four sets of initial conditions (a)  $x(0) = 0.01, y(0) = 0.02, \dot{x}(0) = 0.03, \dot{y}(0) = 0.04$  (blue color) , (b)  $x(0) = 0.01, y(0) = 0.03, \dot{x}(0) = 0.02, \dot{y}(0) = 0.04$  (red color), (c)  $x(0) = 0.02, y(0) = 0.04, \dot{x}(0) = 0.03, \dot{y}(0) = 0.03$  (black color) and (d)  $x(0) = 0.01, y(0) = 0.025, \dot{x}(0) = 0.03, \dot{y}(0) = 0.02$  (green color)

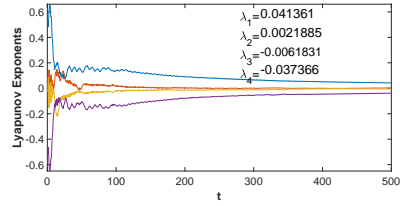
$\mathcal{PT}$ -symmetric case, and depicted in Fig. 12 with only two plots corresponding to non-chaotic and chaotic regions in order to avoid repetition.

## 4 Conclusions & Discussions

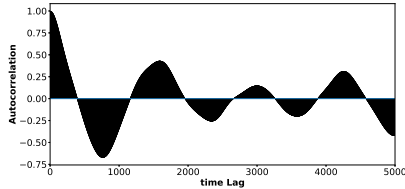
We have investigated two models of coupled VdPD oscillators with balanced loss and gain. The first model is a Hamiltonian system describing a Van der Pol oscillator coupled to another VdPD oscillator through linear as well as nonlinear coupling. The nonlinear coupling is introduced via balanced loss-gain terms. Further, the strength of the linear restoring force for the Van der Pol oscillator depends on the degree of freedom describing the VdPD oscillator. The space-dependent linear restoring force also introduces nonlinearity in the differential equation. The model is a generalization of coupled Duffing oscillator system with balanced loss and gain[12] by allowing the loss-gain terms to be space-dependent. In general, the system is non- $\mathcal{PT}$ -symmetric. The system admits five equilibrium points out of which only three are stable. The co-ordinates of the equilibrium points in the phase-space are different from the coupled Duffing oscillator model[12]. However the stability criteria are same for both the models. The equations of motion are studied by using two different perturbation techniques, namely MSA and RG methods. The approximate solutions in the leading order of the perturbation are identical for both the



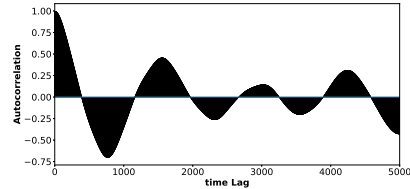
(a) Poincaré section:  $\dot{y}(t)$  VS.  $y(t)$  plot



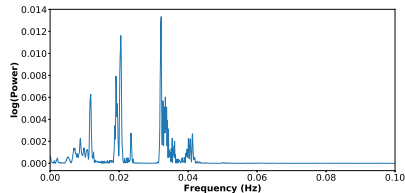
(b) Lyapunov Exponents



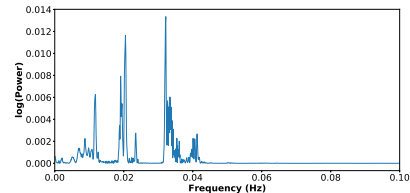
(c) Autocorrelation function of  $x(t)$



(d) Autocorrelation function of  $y(t)$

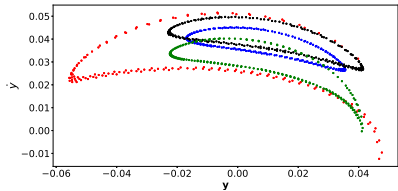


(e) Powerspectra of  $x(t)$

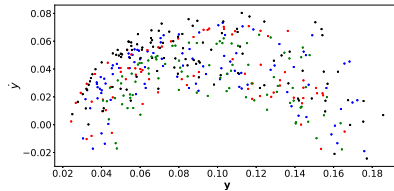


(f) Powerspectra of  $y(t)$

Figure 11: (Color online) Poincaré section, Lyapunov exponents, autocorrelation function and power spectra for  $\Gamma = 0.01, \beta = 1.8, \alpha = 1.0, \tilde{\alpha} = 3.0, a = 1.0, b = 2.0$  with the initial condition  $x(0) = 0.01, y(0) = 0.02, \dot{x}(0) = 0.03, \dot{y}(0) = 0.04$ .



(a)  $\alpha = 1.0, \tilde{\alpha} = 3.0, \beta = 0.85, \Gamma = 0.01, a = 1.0, b = 2.0$



(b)  $\alpha = 1.0, \tilde{\alpha} = 3.0, \beta = 1.05, \Gamma = 0.01, a = 1.0, b = 2.0$

Figure 12: (Color online) Poincaré section of Eq. (47) with four sets of initial conditions (a)  $x(0) = 0.01, y(0) = 0.02, \dot{x}(0) = 0.03, \dot{y}(0) = 0.04$  (blue color), (b)  $x(0) = 0.01, y(0) = 0.03, \dot{x}(0) = 0.015, \dot{y}(0) = 0.04$  (red color), (c)  $x(0) = 0.01, y(0) = 0.04, \dot{x}(0) = 0.025, \dot{y}(0) = 0.03$  (black color) and (d)  $x(0) = 0.01, y(0) = 0.025, \dot{x}(0) = 0.03, \dot{y}(0) = 0.02$  (green color). The parameters  $\alpha = 1.0, \tilde{\alpha} = 3.0, \Gamma = 0.01, a = 1.0, b = 2.0$  are same for both the plots. The parameter  $\beta = 0.85$  for the first plot, while  $\beta = 1.05$  for the second plot.

methods. These solutions are periodic in time with the time-dependence of the amplitudes and phases determined from the RG flow equation. The RG flow equation defines a dimer model and

is exactly solvable for specific initial conditions.

We have investigated the system numerically which confirms the findings of the linear stability analysis and perturbation methods. The system admits regular periodic solution in the  $\mathcal{PT}$ -symmetric as well as non- $\mathcal{PT}$ -symmetric regimes in the parameter-space. The existence of bounded and unbounded solutions in different regimes of the parameter-space is to be understood in terms of the standard techniques of dynamical systems, instead of broken and unbroken phases of  $\mathcal{PT}$  symmetry. The bifurcation diagram exhibits chaotic behaviour in the system beyond a critical value of the linear coupling. There is no external driving force and coupling to the Van der Pol oscillator acts as a source of energy. The model provides yet another example of a Hamiltonian chaos within the ambit of systems with balanced loss and gain. The chaotic behaviour is studied in detail through sensitivity of the solution to the initial conditions, Poincaré-sections, auto-correlation functions and powerspectra. The Lyapunov exponents are computed numerically.

The second model of coupled VdPD oscillators is obtained by modifying the nonlinear interaction in the first model which is a generalization of the models considered in Refs. [1, 33]. The model is non-Hamiltonian for the non-vanishing nonlinear interaction. It describes two damped Duffing oscillators coupled via linear as well as nonlinear coupling. The nonlinear coupling is achieved through the balanced loss-gain terms. The system has  $\mathcal{PT}$  symmetric as well as non- $\mathcal{PT}$ -symmetric regions in the parameter space. We have obtained regular periodic solutions in the  $\mathcal{PT}$  symmetric as well as non- $\mathcal{PT}$ -symmetric regions. The system is chaotic which is investigated through time-series, Poincaré-section, power-spectra, autocorrelation function. The Lyapunov exponents are computed numerically.

The Duffing oscillator, Van der Pol oscillator and their various generalizations have been studied extensively in the literature over several decades with interesting theoretical as well as experimental results. The generalization of these systems by including balanced loss and gain is a recent phenomenon and reveal rich dynamical behaviour. It is expected that further investigations of these new class of systems from different perspectives may shed new insights into hitherto unexplored areas of dynamical systems. A few particular directions of physical interests may be to investigate the quantized versions of these system along with studies on quantum chaos, quantum criticality, quantum synchronizations etc. Some of these issues will be addressed in future.

## 5 Acknowledgements

This work of PKG is supported by a grant (**SERB Ref. No. MTR/2018/001036**) from the Science & Engineering Research Board(SERB), Department of Science & Technology, Govt. of India under the **MATRICES** scheme. The work of PR is supported by CSIR-NET fellowship(**CSIR File No.: 09/202(0072)/2017-EMR-I**) of Govt. of India.

## References

- [1] P. K. Ghosh, Classical Hamiltonian Systems with balanced loss and gain, J. Phys.: Conf. Ser. **2038**, 012012(2021)
- [2] C. M. Bender, M. Gianfreda, S. K. Ozdemir, B. Peng, and L. Yang, Twofold transition in PT-symmetric coupled oscillators, Phys. Rev. A **88**, 062111 (2013).

- [3] B. Peng, S. K. Ozdemir, F. Lei, F. Monifi, M. Gianfreda, G. L. Long, S. Fan, F. Nori, C. M. Bender, and L. Yang, Parity-time-symmetric whispering-gallery microcavities, *Nature Physics* **10**, 394 (2014).
- [4] C. M. Bender, M. Gianfreda and S. P. Klevansky, Systems of coupled PT-symmetric oscillators, *Phys. Rev A* **90**, 022114 (2014).
- [5] I. V. Barashenkov and M. Gianfreda, An exactly solvable  $\mathcal{PT}$ -symmetric dimer from a Hamiltonian system of nonlinear oscillators with gain and loss, *J. Phys. A: Math. Theor.* **47**, 282001(2014).
- [6] D. Sinha and P. K. Ghosh,  $\mathcal{PT}$ -symmetric rational Calogero model with balanced loss and gain, *Eur. Phys. J. Plus* **132**, 460 (2017).
- [7] A. Khare and A. Saxena, Integrable oscillator type and Schrödinger type dimers, *J. Phys. A: Math. Theor.* **50**, 055202 (2017).
- [8] P. K. Ghosh and Debdeep Sinha, Hamiltonian formulation of systems with balanced loss-gain and exactly solvable models, *Annals of Physics* **388**, 276 (2018).
- [9] D. Sinha and P. K. Ghosh, On the bound states and correlation functions of a class of Calogero-type quantum many-body problems with balanced loss and gain, *J. Phys. A: Math. Theor.* **52**, 505203 (2019).
- [10] D. Sinha and P. K. Ghosh, Integrable coupled Liénard-type systems with balanced loss and gain, *Annals of Physics* **400**, 109 (2019).
- [11] Pijush K. Ghosh, Taming Hamiltonian systems with balanced loss and gain via Lorentz interaction : General results and a case study with Landau Hamiltonian, *J. Phys. A: Math. Theor.* **52**, 415202(2019).
- [12] Pijush K. Ghosh and Puspendu Roy, On regular and chaotic dynamics of a non- $\mathcal{PT}$ -symmetric Hamiltonian system of a coupled Duffing oscillator with balanced loss and gain, *J. Phys. A: Math. Theor.* **53**, (2020) 475202.
- [13] O. W. Greenberg, Why is CPT fundamental?, *Found. Phys.* **36**, 1535 (2006).
- [14] P. D. Mannheim, Extension of the CPT theorem to non-Hermitian Hamiltonians and unstable states, *Phys. Lett. B* **753**, 288 (2016).
- [15] R. Krechetnikov and J. E. Marsden, Dissipation-induced instabilities in finite dimensions, *Rev. Mod. Phys.* **79**, 519(2007).
- [16] M. V. Berry and P. Shukla, Hamiltonian curl forces, *Proc. R. Soc. A* **471**, 20150002 (2015); M. V. Berry and P. Shukla, Curl force dynamics: Symmetries, chaos and constants of motion, *New Journal of Physics* **18**, 063018(2016).
- [17] B. van der Pol, LXXXVIII. On “relaxation-oscillations,” *Philos. Mag.* **2**, 978 (1926).
- [18] P. F. Rowat and A. I. Selverston, Modeling the gastric mill central pattern generator of the lobster with a relaxation-oscillator network, *J. Neurophysiology* **70**, 1030(1993).
- [19] R. Fitzhugh, Impulses and Physiological States in Theoretical Models of Nerve Membrane, *Biophysical Journal* **1**, 445 (1961); J. Nagumo, S. Arimoto and S. Yoshizawa, An Active Pulse Transmission Line Simulating Nerve Axon, *Proceedings of the IRE* **50**, 2061 (1962).



- [20] J. C. Lucero and J. Schoentgen, Modeling vocal fold asymmetries with coupled van der Pol oscillators, *Proc. Mtgs. Acoust.* **19**, 060165 (2013).
- [21] J. H. E. Cartwright, V. M. Eguiluz, E. Hernández-García, and O. Piro, Dynamics of elastic excitable media, *Internat. J. Bifur. and Chaos* **9**, 2197 (1999).
- [22] Tony E. Lee and H. R. Sadeghpour, Quantum Synchronization of Quantum van der Pol Oscillators with Trapped Ions, *Phys. Rev. Lett.* **111**, 234101(2013).
- [23] Shovan Dutta and Nigel R. Cooper, Critical Response of a Quantum van der Pol Oscillator, *Phys. Rev. Lett.* **121**, 250401 (2019).
- [24] Helmut R. Brand and Pierre C. Hohenberg and Victor Steinberg, Amplitude equation near a polycritical point for the convective instability of a binary fluid mixture in a porous medium, *Phys. Rev.* **A27** , 591(1983).
- [25] B. J. A. Zielinska, D. Mukamel, V. Steinberg and S. Fishman, Chaotic behavior in externally modulated hydrodynamic systems, *Phys. Rev.* **A32** , 702(1985).
- [26] Yao-Huang Kaon and Ching-Sheu Wang, Analog study of bifurcation structures in a Van der Pol oscillator with a nonlinear restoring force, *Phys. Rev.* **E48**, 2514(1993).
- [27] A. Venkatesan and M. Lakshmanan, Bifurcation and chaos in the double-well Duffing-van der Pol oscillator: Numerical and analytical studies, *Phys. Rev.* **E56**, 6321(1997).
- [28] V. K. Chandrasekar, M. Senthilvelan and M. Lakshmanan, New aspects of integrability of force-free Duffing-van der Pol oscillator and related nonlinear systems, *J. Phys. A: Math. Gen.* **37**, 4527 (2004).
- [29] T. Stachowiak, Hypergeometric first integrals of the Duffing and van der Pol oscillators, *J. Diff. Eqn.* **266**, 5895(2019).
- [30] I. Pastor-Diaz and A. Lopez-Fraguas, Dynamics of two coupled van der Pol oscillators, *Phys. Rev.* **E52**, 1480(1995).
- [31] S. Datta, J. K. Bhattacharjee and D. K. Mukherjee, Higher Dimensional Limit Cycles and Coupling Induced Synchronization in Dynamical Systems, arXiv:2004.10004.
- [32] P. Wofo, J. C. Chedjou and H. B. Fotsin, Dynamics of a system consisting of a van der Pol oscillator coupled to a Duffing oscillator, *Phys. Rev.* **E54**, 5929(1996).
- [33] Jesús Cuevas, Panayotis G. Kevrekidis, Avadh Saxena and Avinash Khare, PT-symmetric dimer of coupled nonlinear oscillators, *Phys. Rev. A* **88**, 032108 (2013).
- [34] A. H. Nayfeh, *Perturbation Methods*, Wiley, 1973; P. K. Jakobsen, Introduction to the method of multiple scales, arXiv:1312.3651.
- [35] Lin Yuan Chen, Nigel Goldenfeld, and Y. Oono, Renormalization Group Theory for Global Asymptotic Analysis, *Phys. Rev. Lett.* **74**, 1889 (1995); L. -Y. Chen, N. Goldenfeld and Y. Oono, The Renormalization group and singular perturbations: Multiple scales, boundary layers and reductive perturbation theory, *Phys. Rev.* **E54**, 376 (1996).
- [36] T. Shah, R. Chattopadhyay, K. Vaidya and S. Chakraborty, Conservative perturbation theory for nonconservative systems, *Phys. Rev. E* **92**, 062927(2015).

- [37] R. Chattopadhyay, T. Shah and S. Chakraborty, Finding the Hannay angle in dissipative oscillatory systems via conservative perturbation theory, *Phys. Rev. E* **97**, 062209 (2018).
- [38] P. G. L. Dirichlet, *Über die Stabilität des Gleichgewichts*, *Crelle* **32**, 85(1846); R. Krechetnikov and J. E. Marsden, Dissipation-induced instabilities in finite dimensions, *Rev. Mod. Phys.* **79**, 519 (2007).
- [39] M. W. Hirsch, S. Smale and R. L. Devany, *Differential Equations, Dynamical Systems, and Introduction to chaos*, Academic Press (2013); N. R. Lebovitz, *Ordinary Differential Equations*, Brook/Cole, 1999 (<http://people.cs.uchicago.edu/~lebovitz/odes.html>).
- [40] U. Singh, A. Raina, V. K. Chandrasekar and D. V. Senthilkumar, Nontrivial amplitude death in coupled parity-time-symmetric Liénard oscillators, *Phys. Rev. E* **104**, 054204 (2021).

This figure "poincare6eps.png" is available in "png" format from:

<http://arxiv.org/ps/2112.10555v2>